

NACA

~~CONFIDENTIAL~~
~~SECURITY INFORMATION~~

RESEARCH MEMORANDUM

HORIZONTAL-TAIL EFFECTIVENESS AND DOWNWASH SURVEYS
FOR TWO 47.7° SWEEPBACK WING-FUSELAGE COMBINATIONS

WITH ASPECT RATIOS OF 5.1 AND 6.0 AT

REYNOLDS NUMBER OF 6.0×10^6

By Reino J. Salmi

Langley Aeronautical Laboratory
Langley Field, Va.

CLASIFICACIÓN CENSO

Reel 1598

of) W. G. W. Date 12-1-3

$$\{5.01, 21, 4, 12, 10, 5\}$$

ASSOCIATION CANCELLED

Authority 224.16.17-3159 Date 11/11/55

By 10/27/2015

CLASSIFIED DOCUMENT

The document contains classified information affecting the National Defense of the United States within the meaning of the Espionage Act, USC 50-31 and 32. Its transmission or the revelation of its contents in any manner to an unauthorized person is prohibited by law.

Information so classified may be imparted only to persons in the military and naval services of the United States, appropriate civilian officers and employees of the Federal Government who have a legitimate interest therein, and to United States citizens of known loyalty and discretion who of necessity must be informed thereof.

NATIONAL ADVISORY COMMITTEE FOR AERONAUTICS

WASHINGTON

January 12, 1951

RESTRICTED

~~CONFIDENTIAL~~

~~SECRET~~

**CONFIDENTIAL**
SECURITY INFORMATION

NATIONAL ADVISORY COMMITTEE FOR AERONAUTICS

RESEARCH MEMORANDUM

HORIZONTAL-TAIL EFFECTIVENESS AND DOWNWASH SURVEYS
FOR TWO 47.7° SWEPTRACK WING-FUSELAGE COMBINATIONS

WITH ASPECT RATIOS OF 5.1 AND 6.0 AT A

REYNOLDS NUMBER OF 6.0×10^6

By Reino J. Salmi

SUMMARY

An experimental investigation of the effectiveness of a horizontal tail on two 47.7° sweptback wing-fuselage combinations of aspect ratios 5.1 and 6.0 was made at a Reynolds number of 6.0×10^6 and a Mach number of 0.14. The tests were made with various combinations of leading-edge flaps, drooped-nose, split flaps, and double slotted flaps in addition to the flaps-neutral configurations. Air-stream surveys in the region of the tail were also made.

The results corroborate previous low-speed investigations in that a tail position just below the extended wing-chord plane maintained effectiveness and improved the stability at the high angles of attack whereas a tail position well above the extended wing-chord plane was unfavorable. Although the low tail increased the stability of the flaps-neutral combinations at the very high angles of attack, it did not reduce the large unstable change in dC_m/dC_L (rate of change of pitching-moment coefficient with lift coefficient) which occurred at an angle of attack of 13° . The initial unstable variations of dC_m/dC_L which occurred at moderately high lift coefficients for the combinations with the leading- and trailing-edge flaps deflected was eliminated by the low tail for trailing-edge-flap spans extending to 0.400 semispan. For trailing-edge-flap spans extending to 0.500 semispan and for combinations with only the leading-edge flaps deflected, the initial unstable variations of dC_m/dC_L were considerably reduced.

INTRODUCTION

Previous experimental investigations of the effects of horizontal-tail position on the low-speed static longitudinal stability characteristics

~~CONFIDENTIAL~~
~~SECURITY INFORMATION~~

of sweptback-wing models (references 1, 2, and 3) have shown that the stability exhibited at high lift coefficients is critically dependent on the vertical location of the horizontal tail. It has been shown that the optimum tail position from the point of view of low-speed stability takes advantage of the favorable downwash gradients below the wake center line. Reference 4 shows that for two wings of 47.7° sweepback at the leading edge and aspect ratios of 5.1 and 6.0, the longitudinal instability caused by tip stall could be alleviated by the use of leading-edge devices, but, for some combinations of leading- and trailing-edge flaps, unstable variations of the pitching moment would occur prior to the maximum lift.

The present investigation was conducted, therefore, to determine the longitudinal stability characteristics of the two 47.7° sweptback wings in combination with a fuselage and horizontal tail and to determine the extent to which the horizontal tail is effective in overcoming the unstable variations of the pitching moment prior to the maximum lift. The tests were made at a Reynolds number of about 6.0×10^6 (Mach number of 0.14). Air-stream surveys of the flow in the region of the tail were also made.

SYMBOLS

C_L	lift coefficient (Lift/ qS)
C_m	pitching-moment coefficient about $0.25\bar{c}$ (Pitching moment/ $qS\bar{c}$)
S	wing area
S_t	tail area
\bar{c}	mean aerodynamic chord $\left(\frac{2}{3} \int_0^{b/2} c^2 dy \right)$
c	wing chord
c_t	tail chord
c'	wing chord normal to 0.286-chord line
b	wing span
b_t	tail span
y	lateral distance from plane of symmetry
q	free-stream pressure $\left(\frac{1}{2} \rho V^2 \right)$

ρ	mass density of air
V	free-stream velocity
q_t	dynamic pressure at tail
ϵ	downwash angle, degrees
σ	sidewash angle, positive when angle of attack of vertical tail is decreased at positive yaw angles, degrees
α	angle of attack referred to root-chord line, degrees
$d\epsilon/d\alpha$	rate of change of downwash angle with angle of attack
dC_m/dC_L	rate of change of pitching-moment coefficient with lift coefficient
τ	tail-effectiveness parameter $\left(\frac{dC_{m_t}/d\alpha}{\frac{S_t}{S} \frac{l}{c} C_{L_{\alpha_t}}} \right)$
$dC_{m_t}/d\alpha$	rate of change of pitching moment due to tail with angle of attack
$C_{m_{i_t}}$	rate of change of pitching moment with tail incidence angle
$(C_{m_{i_t}})_0$	value of $C_{m_{i_t}}$ at zero lift for high tail position with wing flaps neutral
$C_{L_{\alpha_t}}$	lift-curve slope of isolated tail, 0.0497 per degree
l	tail length, distance from $0.25\bar{c}$ of wing to $0.25\bar{c}$ of tail
i_t	tail incidence angle referred to wing-chord line
δ_n	drooped-nose deflection angle
z	tail height, measured normal to wing-chord plane
z'	distance from wing-chord plane measured parallel to vertical axes of tunnel
η	tail efficiency factor, ratio of $(C_{m_{i_t}})_0$ of any tail position to $(C_{m_{i_t}})_0$

Subscripts:

e	effective value, value based on force data
t	tail
w	wing
av	average value, value obtained from air-flow surveys
0	value at zero wing lift

MODEL

The geometric characteristics of the models are presented in figure 1. The wings had 47.7° sweepback at the leading edge and aspect ratios of 5.1 and 6.0 which were obtained by interchangeable wing tips. The corresponding taper ratios were 0.383 and 0.313, respectively, and NACA 64-210 airfoil sections were employed normal to the 0.286-chord line. The wings had no dihedral but 1.32° and 1.72° of washout existed for the wings of aspect ratios 5.1 and 6.0, respectively.

The horizontal tail had 42.05° sweepback at the leading edge, an aspect ratio of 4.01, a taper ratio of 0.625, and NACA 0012-64 airfoil sections parallel to the plane of symmetry. The tail height is defined as the perpendicular distance between the wing-chord plane extended and the 0.25 \bar{c} point of the tail (see fig. 1). The incidence of the tail is referred to the wing root-chord line and was changed by rotation about the 0.25 \bar{c} point of the tail.

The circular fuselage had a fineness ratio of 11.0. An incidence angle of 2° existed between the fuselage center line and the wing root-chord line.

The geometry of the leading-edge and trailing-edge flaps is presented in figure 2. The split flaps were equal to 20 percent of the wing chord normal to the 0.286-chord line and were deflected 60° as measured in a plane normal to the 0.286-chord line. The split flaps extended to $0.400b/2$ and $0.500b/2$ on the wing of aspect ratio 5.1 and to $0.449b/2$ on the wing of aspect ratio 6.0. The double-slotted-flap chord was equal to 25 percent of the wing chord normal to the 0.286-chord line and a deflection angle of 50° was maintained in a plane normal to the 0.286-chord line. Double slotted flaps extending to $0.400b/2$ were used on the wing for $A = 5.1$ and to $0.462b/2$ on the wing for $A = 6.0$.

The leading-edge flaps had a constant chord of 3.05 inches normal to the leading edge and were deflected 45° from the wing-chord plane measured in a plane normal to the leading edge. Leading-edge-flap spans

of $0.475b/2$ and $0.525b/2$ were used on the wing for $A = 5.1$ and a span of $0.481b/2$ was tested on the wing for $A = 6.0$. The drooped nose was hinged on the wing lower surface at the 16-percent-chord line of the sections normal to the 0.286-chord line and was deflected 20° about the hinge line. The drooped-nose span was $0.375b/2$.

TESTS

The tests were conducted in the Langley 19-foot pressure tunnel with the air compressed to approximately 33.5 pounds per square inch absolute. The data were obtained at a Reynolds number of about 6.0×10^6 and a Mach number of 0.14. Figure 3 shows one of the wing-fuselage-tail combinations mounted in the tunnel.

The aerodynamic forces and moments were measured through an angle-of-attack range for the various combinations tested. The air-stream surveys were made in a plane normal to the tunnel center line at a point which was located between the extreme forward and rearward locations of the 0.25C of the tail (see fig. 4). The measurements of the downwash angles, sidewash angles, and dynamic pressures were obtained by using a 6-tube rake as shown in figure 5.

In the following discussion, the tail positions equal to 38.2- and 34.3-percent semispan above the extended wing-chord plane for the wings having aspect ratios 5.1 and 6.0 are referred to as the high position, and the tail positions 5.3- and 4.8-percent semispan below the extended wing-chord plane are referred to as the low position. An intermediate position of 15.0-percent semispan above the extended wing-chord plane was tested for only one combination on the wing of aspect ratio 5.1.

Table I may be used as a guide to the various combinations of leading- and trailing-edge flaps and horizontal-tail arrangements that were tested.

REDUCTION OF DATA

The data presented herein have been corrected for air-stream misalignment, support tare and interference effects, and jet-boundary effects. The jet-boundary corrections for the angle of attack, drag coefficient, and pitching-moment coefficient were obtained by a method based on reference 5. The jet-boundary corrections were also applied to the air-flow-survey data and consist of an angle change to the downwash and a downward displacement to the field of flow.

Average values of downwash and dynamic pressure.- The average values of the dynamic-pressure ratio and the downwash angle in the region of the

tail were obtained by weighting the measured values from the air-flow surveys according to the following equations:

$$\left(\frac{q_t}{q}\right)_{av} = \frac{2}{S_t} \int_0^{b_t/2} \frac{q_t}{q} c_t dy$$

and

$$\epsilon_{av} = \frac{2}{S_t \left(\frac{q_t}{q}\right)_{av}} \int_0^{b_t/2} \frac{q_t}{q} \epsilon c_t dy$$

Effective values of downwash and dynamic pressure.- Isolated-tail tests showed a constant lift-curve slope through the angle-of-attack range (reference 1); thus, the computations of the effective downwash angle and dynamic-pressure ratios were simplified to

$$\eta \left(\frac{q_t}{q}\right)_e = \frac{C_{m_{l_t}}}{(C_{m_{l_t}})_0}$$

and

$$\epsilon_e = \alpha + i_t - \alpha_t$$

where

$$\alpha_t = \frac{C_{m_t}}{C_{m_{l_t}}}$$

Tail efficiency factor.- In order to compare the effective values of q_t/q to the average values, the tail efficiency factor η was estimated from the pitching-moment data. The factor η was based on the rate of change of pitching moment with tail incidence angle. The interference effects for the high tail position were assumed to be negligible and, with the wing flaps neutral, the dynamic-pressure ratio at zero lift

for the high tail was assumed to be about 1.0. The efficiency factor η was then obtained from the relation

$$\eta = \frac{(C_{m_{1t}})_0}{(C_{m_{1t}})_0'}$$

where the prime refers to the value for the high tail with the flaps neutral.

The following table presents the values of $C_{m_{1t}}$ at zero lift used to obtain the tail efficiency factor for the various combinations and tail positions:

Model configuration	High tail		Low tail	
	$(C_{m_{1t}})_0$	η (percent)	$(C_{m_{1t}})_0$	η (percent)
Flaps neutral	0.0205	100.0	0.0172	83.9
0.475b/2 leading-edge flaps	.0213	103.9	.0173	84.4
0.400b/2 split flaps and 0.475b/2 leading-edge flaps	.0205	100.0	.0180	87.8
0.400b/2 double slotted flaps and 0.475b/2 leading-edge flaps	.0211	102.9	.0174	84.9

The accuracy of the values of $(C_{m_{1t}})_0$ depends on the accuracy of measuring the tail incidence angle, the pitching moment, and also on the dynamic-pressure ratio at the tail which may not be unity at zero lift. The accuracy of the tail incidence angle is believed to be within 0.2° for each setting.

Tail effectiveness parameter.- In order to compare the effectiveness of the tail for the various combinations of leading- and trailing-edge flaps on the wing, it is convenient to use a tail effectiveness factor τ (reference 3) which accounts for the effects of both the downwash and the dynamic pressure. The factor τ is defined as follows:

$$\tau = - \left[\left(1 - \frac{d\epsilon}{d\alpha} \right) \frac{q_t}{q} + \alpha_t \frac{d(q_t/q)}{d\alpha} \right] \eta \quad (1)$$

where

$$\alpha_t = \alpha + i_t - \epsilon$$

or

$$\tau = \frac{\left(\frac{dC_{m_t}}{d\alpha}\right)_{\text{measured}}}{\frac{S_t}{S} \frac{l}{c} C_{L\alpha_t}} = \frac{\left(\frac{dC_{m_t}}{d\alpha}\right)_{\text{measured}}}{(C_{m_{i_t}})_0} \quad (2)$$

Equation (1) shows that, when $\frac{d(q_t/q)}{d\alpha}$ is zero, the values of τ are independent of tail load and hence are applicable to any degree of trim or to any center-of-gravity location. The values of τ presented herein were obtained with a fixed tail incidence, and large out-of-trim conditions existed at the higher lift coefficients. Through the angle-of-attack range for which the tail passes through the wake, finite values of $\frac{d(q_t/q)}{d\alpha}$ are obtained; hence the values of τ through that angle-of-attack range are more nearly representative of the center-of-gravity location at which the measured tail load would provide trim at the wake center.

RESULTS AND DISCUSSION

Presentation of Results

The main results of the investigation are summarized in table I. The basic force data and resulting tail effectiveness parameters are presented in figures 6 to 23. The effectiveness of the tail for various spans of leading-edge flaps and trailing-edge split flaps is shown in figure 24. Figures 25 to 28 present contours of the air-flow characteristics in the region of the tail. A comparison of the downwash angles and dynamic-pressure ratios obtained from the air-flow surveys and the force data is given in table II.

Effects of Tail Position on the Tail

Effectiveness and Stability

In general, the results of the present investigation corroborate those reported in references 1 and 2. Some improvement in the stability in the high-lift range was obtained for all the combinations tested when the tail was located below the extended wing-chord plane whereas a tail location well above the extended wing-chord plane decreased the stability for most of the combinations. The reduced tail effectiveness for the low tail position at low angles of attack which results from fuselage interference was also evident (see table II).

Plain wings.- With the flaps neutral, the effectiveness of the tail in the low position was constant through most of the angle-of-attack range with an increase in the stabilizing effect occurring at the very high angles of attack for both the wings of aspect ratios 5.1 and 6.0 (figs. 6 to 9). In the high position, the tail exhibited a loss of effectiveness at the moderately high angles of attack and became destabilizing at an angle of attack of 16° (figs. 7 and 9). The increase in the effectiveness of the low tail at the high angles of attack may be attributed mainly to a decrease in the rate of change of downwash at the tail $d\epsilon_e/d\alpha$, whereas the destabilizing effect of the high tail resulted from a large increase of $d\epsilon_e/d\alpha$ in the high angle-of-attack range.

Although the low tail increased the stability of the flaps-neutral combinations near the maximum lift coefficient, the severe instability which occurred at an angle of attack of 13° was not reduced (figs. 6 and 8). The maximum usable wing lift coefficient (prior to the wing stall) of about 0.85 was not appreciably increased by the tail.

Leading-edge devices and trailing-edge flaps deflected.- The tail effectiveness for both the high and low positions with the various flap configurations was about the same as for the flaps-neutral combination. With only the leading-edge flaps deflected (figs. 10 to 13), the effectiveness of the low tail was increased at the high angles of attack primarily by a decrease of $d\epsilon_e/d\alpha$. Figures 11 and 13 show that the high tail was destabilizing through most of the high angle-of-attack range because of a large increase of $d\epsilon_e/d\alpha$ but, at the very highest angles of attack, $d\epsilon_e/d\alpha$ returned to a small value with a resulting increase in the tail effectiveness although a large decrease of $\eta(q_t/q)_e$ occurred. The longitudinal instability prior to the maximum lift coefficient was considerably reduced but not completely eliminated by the low tail, as indicated by figures 10 and 12.

With the split flaps and leading-edge flaps deflected, the values of τ for the low tail position indicated an increase in effectiveness

in the angle-of-attack range from about 8° to 16° for the wing with an aspect ratio 5.1 and 12° to 16° for the wing of aspect ratio 6.0 which resulted from a decrease of $d\epsilon_e/d\alpha$.

When the double slotted flaps and leading-edge flaps were deflected, the effectiveness of the low tail for the wing of aspect ratio 5.1 decreased with increasing angle of attack up to about 8° , beyond which a large increase in effectiveness with increasing angle of attack occurred up to about 12° (fig. 19). The initial decrease of τ was not evident for the wing of aspect ratio 6.0 (fig. 21) and the increase in effectiveness was more gradual. The marked influence of $d\epsilon_e/d\alpha$ on τ as compared to the effect of $\eta(q_t/q)_e$ can be seen from figures 19 and 21, which show that the destabilizing effect of the high tail increased in the angle-of-attack range between 8° and 17° because of a corresponding increase of $d\epsilon_e/d\alpha$, but that beyond 17° τ decreased in its positive value and again became negative at an angle of attack of about 23° although a large decrease of $\eta(q_t/q)_e$ occurred. An intermediate tail position of $0.15b/2$ above the extended wing-chord plane was tested on the wing of aspect ratio 5.1. The results were similar to those of the high tail position except that τ did not become positive and an appreciable increase in the tail effectiveness occurred at the high angles of attack (fig. 19). When the $0.375b/2$ drooped nose was used in combination with the double slotted flaps on the wing of aspect ratio 5.1, the results were essentially the same as when the $0.475b/2$ leading-edge flaps were used (fig. 23). The increase in tail effectiveness at moderate angles of attack for the low position was somewhat greater with the drooped nose.

As pointed out in reference 4, many of the leading-edge- and trailing-edge-flap combinations which exhibited stable pitching-moment breaks at the maximum lift coefficient experienced unstable variations of the pitching moment prior to the maximum lift. Figure 24 presents the results of tests made to determine the effect of the tail in the low position for the wing-fuselage combination with various spans of split flaps and leading-edge flaps which have various degrees of instability prior to the maximum lift. Figure 24 shows that with the $0.400b/2$ split flaps deflected, the initial instability prior to the maximum lift, as indicated by the change of dC_m/dC_L to a more positive value, was eliminated by the tail in the low position for both the $0.475b/2$ and $0.525b/2$ leading-edge flaps. With the $0.500b/2$ split flaps, however, the initial instability prior to the maximum lift was reduced somewhat but not eliminated by the tail. From the pitching-moment characteristics of all the combinations with either $0.400b/2$ split or double slotted flaps (figs. 14, 18, and 22), it can also be shown that the low tail eliminates the undesirable changes of dC_m/dC_L which occur in the angle-of-attack range from about 9° to 12° . The effectiveness of the low tail is, therefore, sensitive to changes in the span of the trailing-edge flaps but appears to be relatively unaffected by the type or span (for the limits tested herein) of the leading-edge devices.

Figure 24 indicates that the effectiveness of the low tail in eliminating the instability with the 0.400b/2 split flaps may be due to the decrease in $d\epsilon_e/d\alpha$ which occurred at approximately the same angle of attack as the forward shift of the aerodynamic center of the tail-off configuration, whereas with the 0.500b/2 split flaps the decrease of $d\epsilon_e/d\alpha$ seemed to occur at an angle of attack which was larger than that at which the unstable change in dC_m/dC_L occurred. The air-flow surveys of figure 27 indicate that the tip sections of the tail emerge first from the region above the wake center line, and, for the trailing-edge flap spans greater than 0.400b/2, the region of the lowered wake center line behind the flaps may be broader; thereby, the stabilizing effect of the tail is delayed.

Effects of Trim on τ

As previously indicated, the values of τ were obtained with a fixed tail incidence and a large out-of-trim condition existed at the high lift coefficients. The effects on τ of changes in the tail load were therefore calculated and found to be of significant magnitude. The changes in τ were greatest for the combinations with double slotted flaps because of the large tail load required for trim and the deep wake behind the flaps. The effects on τ of the changes in α_t required for trimming are shown in figure 19 for the wing of aspect ratio 5.1 with 0.400b/2 double slotted flaps and 0.475b/2 leading-edge flaps deflected. Inasmuch as a negative value of α_t was required for trim, an increase in q_t/q resulted in a reduction of the tail effectiveness and a decrease in q_t/q increased the tail effectiveness. The changes in τ were significant only at the high angles of attack which correspond to the lift range where the lift-curve slope is small. It has been found that through the angle-of-attack range for which the values of $\frac{d(q_t/q)}{d\alpha}$ of the present wing are maximum, the values of τ are applicable to a trim condition for a center-of-gravity location rearward of the 25-percent \bar{c} .

Air-Flow Surveys

The advantages of locating the horizontal tail in the region below the wing wake for improving the low-speed stability of the wing-fuselage-tail combinations at the higher angles of attack can also be shown from an analysis of the contour charts of the air-flow characteristics (figs. 25 to 28). In using the contour charts to obtain the average values of q_t/q and ϵ for comparison with the effective values, discrepancies in the average values may result from the following causes: (1) The survey plane was perpendicular to the tunnel center line (see fig. 4), and, because of the tail sweepback and the forward and rearward movement of the tail with angle of attack, the tail sections may be located at stations in the flow

field different from those used in the calculations so that greatly different average values result where the q_t/q and ϵ gradients are large: (2) where the values of q_t/q and ϵ were very large, extrapolations of the survey-rake calibrations were necessary (noted by shaded areas on contour charts); and (3) no survey data were obtained in the region directly below the fuselage. The comparison of the effective and average values of ϵ and q_t/q in table II shows that, in general, fairly good agreement was obtained for the high tail position and somewhat poorer agreement for the low tail.

Inasmuch as the low tail did not reduce the unstable shift of the aerodynamic center prior to the maximum lift for the flaps-neutral combinations, a brief investigation was made by using the contour charts to determine whether a more favorable tail location than the low position would be indicated. The results indicated that a tail position of $0.05b/2$ above the extended wing-chord plane was at least as good as the low position ($-0.05b/2$) that was tested but that any further increases in the stability of the wing-fuselage-tail combination would be small. Fairly good agreement between the calculated and experimental pitching-moment curves for the low tail position was obtained.

The contour charts indicate strong vorticity in the region of the tail at the high angles of attack. Large negative sidewash angles which developed in the region about 40- to 50-percent semispan above the extended wing-chord plane decreased as the extended wing-chord plane was approached and finally assumed large positive values. References 4 and 6 pointed out that a vortex flow developed along the leading edge of the subject wings and that, at high angles of attack, the vortex flow was concentrated over the inboard areas of the wings. The increased vorticity near the tail may, therefore, be caused by a more rapid rolling up of the vortex sheet due to the strong vortices formed at the leading edge. The vortex flow was not evident on a wing of lower sweepback (42° , reference 1), and relatively smaller sidewash angles were obtained in the region of the tail (reference 7). With the leading-edge flaps deflected, both the downwash and sidewash angles are decreased at the high angles of attack.

The large depression of the wake center line due to the trailing-edge flaps for the region directly behind the flaps can be seen from the contour charts. As the wake center line moves above the wing-chord plane with increasing angle of attack, only the tip sections of the high tail may be at the wake center, but the entire tail may be adversely affected by the broad wake. The location of the trailing vortices from the split and double slotted flaps can also be determined from the contour charts. The vortex from the trailing-edge flaps moved from a position well below the extended wing-chord plane to a point considerably above the extended wing-chord plane when the angle of attack was increased.

CONCLUDING REMARKS

The main results of the investigation of the effectiveness of a horizontal tail on two 47.7° sweptback wing-fuselage combinations of aspect ratios 5.1 and 6.0 are summarized as follows:

The low tail increased the stability of the flaps-neutral combinations at the very high angles of attack but it did not reduce the large unstable change of dC_m/dC_L (rate of change of pitching-moment coefficient with lift coefficient) which occurred at an angle of attack of 13° . Calculations based on the air-flow surveys indicated that a tail position just above the wing-chord plane was as effective as the low position when the wing flaps were neutral. The relatively smaller unstable variations of the pitching moment which occurred at moderately high lift coefficients on the combinations with the leading- and trailing-edge flaps deflected were eliminated by the low tail for trailing-edge flaps extending to 0.400 semispan and were considerably reduced for trailing-edge flap spans extending to 0.500 semispan and for combinations with only the leading-edge flaps deflected. The high tail position was destabilizing at the high angles of attack for all the combinations tested.

Langley Aeronautical Laboratory
National Advisory Committee for Aeronautics
Langley Field, Va.

REFERENCES

1. Spooner, Stanley H., and Martina, Albert P.: Longitudinal Stability Characteristics of a 42° Sweptback Wing and Tail Combination at a Reynolds Number of 6.8×10^6 . NACA RM L8E12, 1948.
2. Foster, Gerald V., and Fitzpatrick, James E.: Longitudinal-Stability Investigation of High-Lift and Stall-Control Devices on a 52° Sweptback Wing with and without Fuselage and Horizontal Tail at a Reynolds Number of 6.8×10^6 . NACA RM L8I08, 1948.
3. Foster, Gerald V., and Griner, Roland F.: A Study of Several Factors Affecting the Stability Contributed by a Horizontal Tail at Various Vertical Positions on a Sweptback-Wing Airplane Model. NACA RM L9H19, 1949.
4. Salmi, Reino J.: Effects of Leading-Edge Devices and Trailing-Edge Flaps on the Longitudinal Characteristics of Two 47.7° Sweptback Wings of Aspect Ratios 5.1 and 6.0 at a Reynolds Number of 6.0×10^6 . NACA RM L50F20, 1950.
5. Eisenstadt, Bertram J.: Boundary-Induced Upwash for Yawed and Swept-Back Wings in Closed Circular Wind Tunnels. NACA TN 1265, 1947.
6. Salmi, Reino J., and Carros, Robert J.: Longitudinal Characteristics of Two 47.7° Sweptback Wings with Aspect Ratios of 5.1 and 6.0 at Reynolds Numbers up to 10×10^6 . NACA RM L50A04, 1950.
7. Furlong, G. Chester, and Bollech, Thomas V.: Downwash, Sidewash, and Wake Surveys behind a 42° Sweptback Wing at a Reynolds Number of 6.8×10^6 with and without a Simulated Ground. NACA RM L8G22, 1948.

TABLE I.- SUMMARY OF TAIL EFFECTIVENESS AND PITCHING-MOMENT CHARACTERISTICS
OF TWO 47.7° SWEEPBACK WING-FUSELAGE-TAIL COMBINATIONS

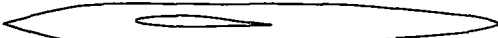
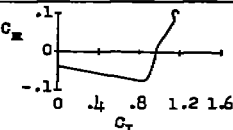


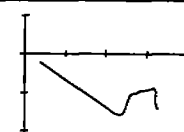
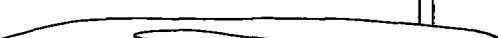
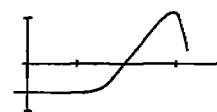

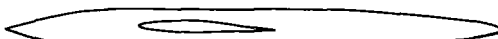
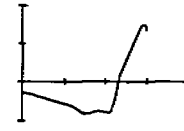
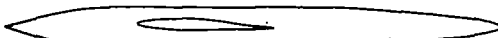
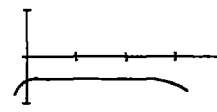
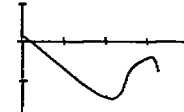

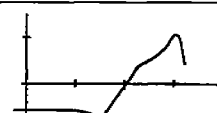

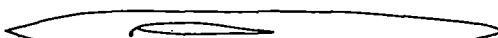
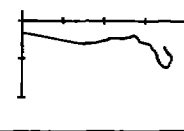
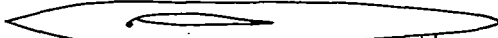
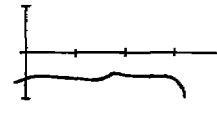
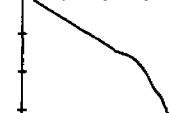
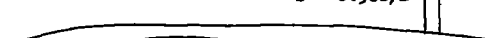
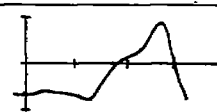
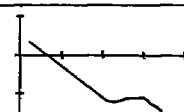
Model configuration and tail height, z , above extended wing-chord plans	Tail effectiveness parameter, τ	C_m characteristics	Figure referring to τ
$A = 5.1$ Tail off  Plain wing			
 $z = -0.05b/2$			7(a)
 $z = 0.38b/2$			7(b)
$A = 6.0$ Tail off  Plain wing			
 $z = -0.05b/2$			9(a)
 $z = 0.34b/2$			9(b)
$A = 5.1$ Tail off  $0.475b/2$ leading-edge flap			
 $z = -0.05b/2$			11(a)
 $z = 0.38b/2$			11(b)

TABLE I.- SUMMARY OF TAIL EFFECTIVENESS AND PITCHING-MOMENT CHARACTERISTICS
OF TWO 47.7° SWEEPBACK WING-FUSELAGE-TAIL COMBINATIONS - Continued


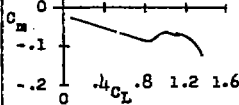

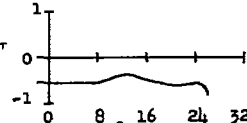
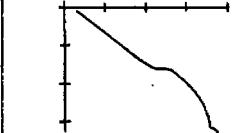
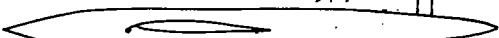
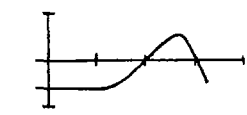
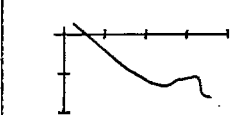
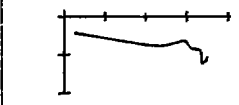

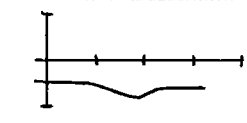
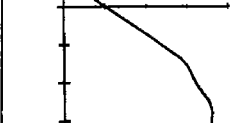

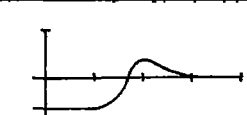
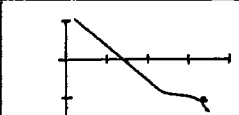
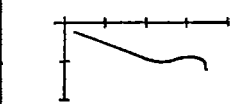

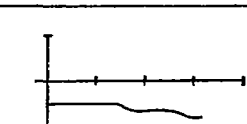
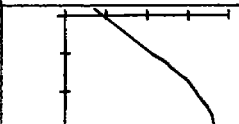

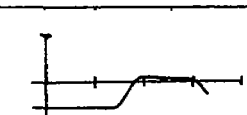
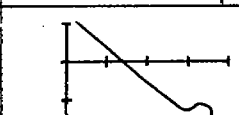
Model configuration and tail height, z , above extended wing-chord plane	Tail effectiveness parameter, τ	C_m characteristics	Figure referring to
$A = 6.0$ Tail off  $0.481b/2$ leading-edge flap			
 $z = -0.05b/2$			13(a)
 $z = 0.34b/2$			13(b)
$A = 5.1$ Tail off $0.475b/2$ leading-edge flap $0.400b/2$ split flap			
 $z = -0.05b/2$			15(a)
 $z = 0.38b/2$			15(b)
$A = 6.0$ Tail off $0.481b/2$ leading-edge flap $0.449b/2$ split flap			
 $z = -0.05b/2$			17(a)
 $z = 0.34b/2$			17(b)

TABLE I.- SUMMARY OF TAIL EFFECTIVENESS AND PITCHING-MOMENT CHARACTERISTICS
OF TWO 47.7° SWEEPBACK WING-FUSELAGE-TAIL COMBINATIONS - Concluded


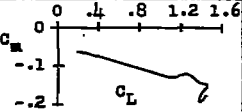

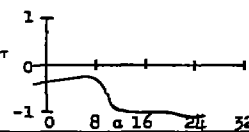
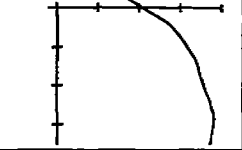

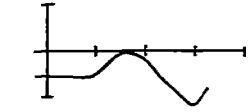
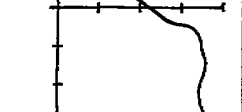

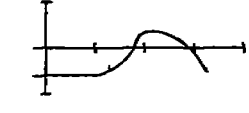
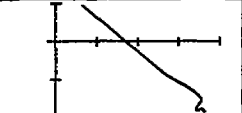

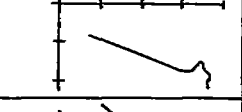

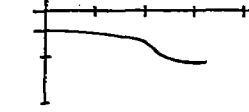
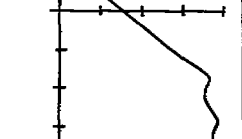

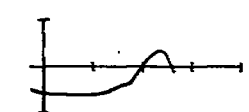
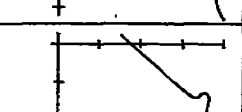

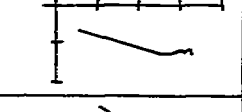

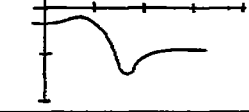
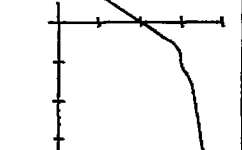

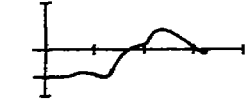
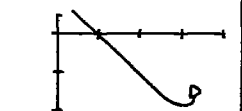
Model configuration and tail height, z , above extended wing-chord plane	Tail effectiveness parameter, τ	C_m characteristics	Figure referring to τ
$A = 5.1$ Tail off  $0.475b/2$ leading-edge flap $0.400b/2$ double slotted flap			
 $z = -0.05b/2$			19(a)
 $z = 0.15b/2$			19(b)
 $z = -0.38b/2$			19(b)
$A = 6.0$ Tail off  $0.481b/2$ leading-edge flap $0.462b/2$ double slotted flap			
 $z = -0.05b/2$			21(a)
 $z = 0.34b/2$			21(b)
$A = 5.1$ Tail off  $0.375b/2$ drooped-nose, $\theta_n = 20^\circ$ $0.400b/2$ double slotted flap			
 $z = -0.05b/2$			23(a)
 $z = 0.38b/2$			23(b)

TABLE II.- COMPARISON OF AVERAGE AND EFFECTIVE VALUES OF THE DOWNWASH ANGLES AND DYNAMIC-PRESSURE

RATIOS AT THE TAIL AND TAIL EFFICIENCY FACTORS FOR A 47.7° SWEEPBACK WING-FUSELAGE

COMBINATION OF ASPECT RATIO 5.1

Model configuration	α (deg)	$z = 0.38\frac{b}{2}$					$z = -0.05\frac{b}{2}$				
		$\left(\frac{q_t}{q}\right)_{av}$	$\left(\frac{q_t}{q}\right)_e$	η (percent)	ϵ_{av} (deg)	ϵ_e (deg)	$\left(\frac{q_t}{q}\right)_{av}$	$\left(\frac{q_t}{q}\right)_e$	η (percent)	ϵ_{av} (deg)	ϵ_e (deg)
Flaps neutral	4.4	1.02	1.00	100.0	2.8	3.2	0.99	1.02	83.9	1.2	0.6
	8.6	1.02	1.00	100.0	4.5	4.9	.97	1.02	83.9	3.3	2.4
	14.9	1.04	1.00	100.0	7.8	8.0	1.03	1.03	83.9	5.2	5.7
	19.0	1.05	1.00	100.0	12.5	13.0	1.04	1.03	83.9	6.1	6.9
	23.1	1.08	1.00	100.0	20.8	20.8	1.05	1.03	83.9	6.7	8.3
0.475b/2 leading-edge flaps	4.4	1.03	.99	103.9	2.7	3.3	1.01	1.01	84.4	1.2	.2
	8.6	1.03	1.00	103.9	4.4	4.8	1.01	1.05	84.4	3.1	2.1
	15.0	1.03	1.00	103.9	7.7	8.5	1.01	1.03	84.4	5.0	4.2
	19.1	1.03	1.00	103.9	13.6	13.6	1.02	1.04	84.4	6.1	6.5
	23.2	.91	.78	103.9	20.0	19.1	1.03	1.08	84.4	6.5	8.8
0.400b/2 split flaps and 0.475b/2 leading-edge flaps	4.6	1.04	1.03	100.0	4.5	5.1	.89	.98	87.8	3.8	2.7
	8.8	1.04	1.03	100.0	6.1	6.6	.90	1.01	87.8	6.3	4.6
	15.1	1.04	1.05	100.0	10.0	10.9	.96	1.02	87.8	6.6	6.1
	19.2	1.04	.94	100.0	15.6	15.5	1.01	1.02	87.8	6.1	7.1
	23.2	.89	.82	100.0	21.1	19.2	1.03	1.02	87.8	5.0	8.2
0.400b/2 double slotted flaps and 0.475b/2 leading-edge flaps	4.8	1.05	1.00	102.9	5.7	6.3	.91	.94	84.9	12.5	8.2
	9.0	1.04	1.00	102.9	8.2	8.2	.91	.94	84.9	13.3	10.8
	15.3	1.05	.97	102.9	12.1	12.3	.80	.95	84.9	11.9	10.1
	19.3	.99	.80	102.9	17.8	16.9	.94	.99	84.9	7.4	9.2
	23.3	.67	.58	102.9	27.9	21.4	.97	1.12	84.9	10.0	9.9

NACA

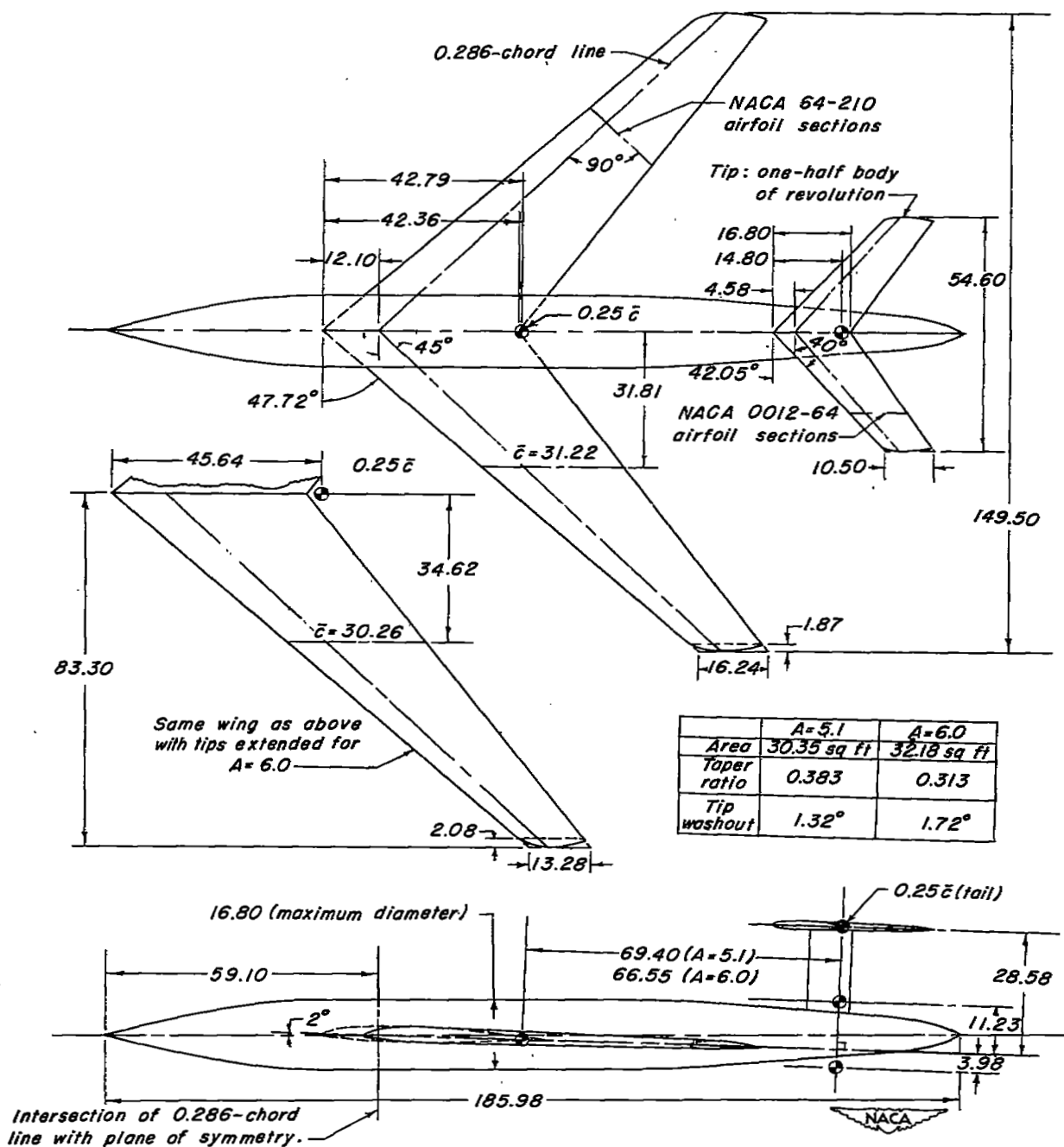


Figure 1.- Geometry of the 47.7° sweptback wing-fuselage and tail combinations. All dimensions are in inches.

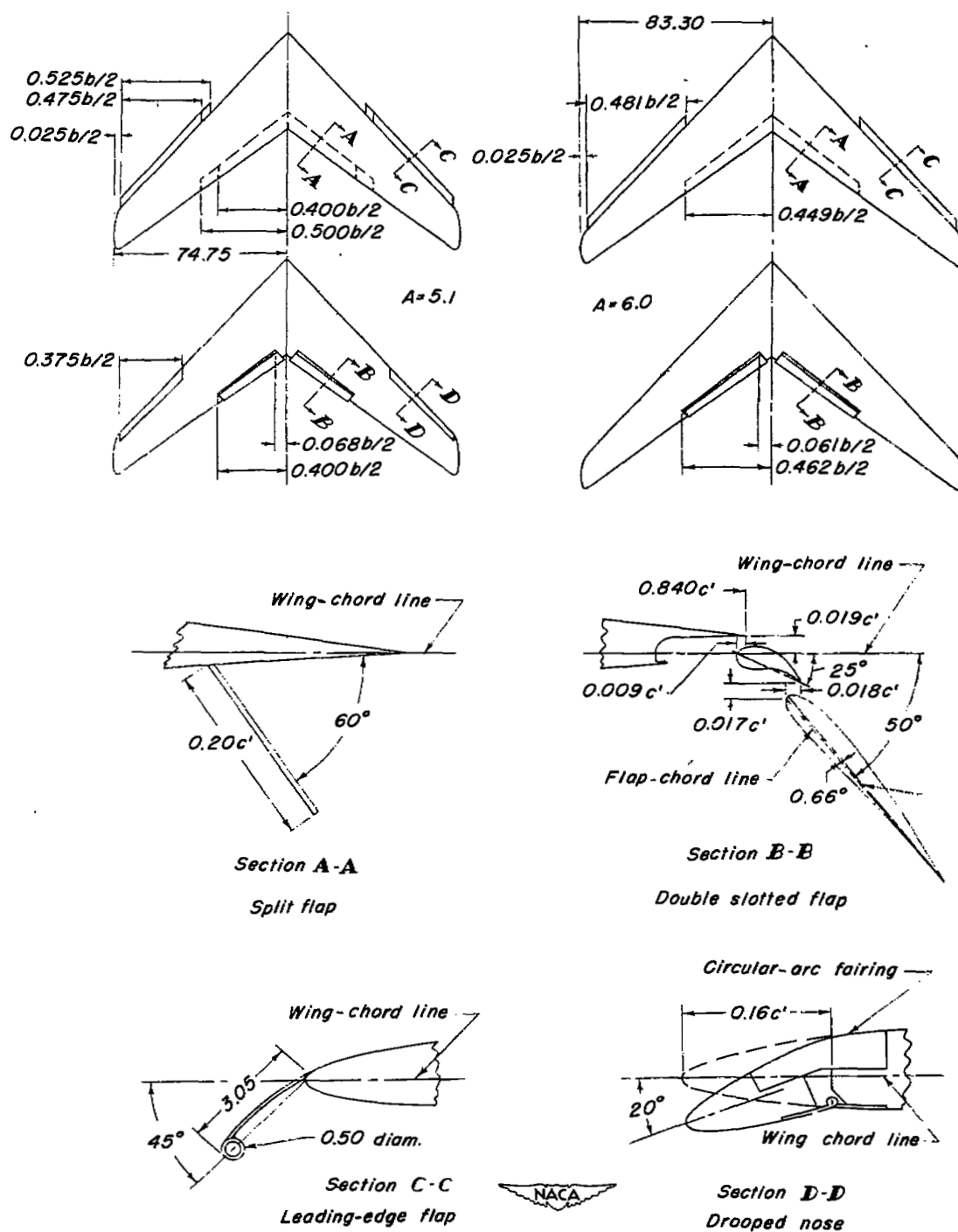
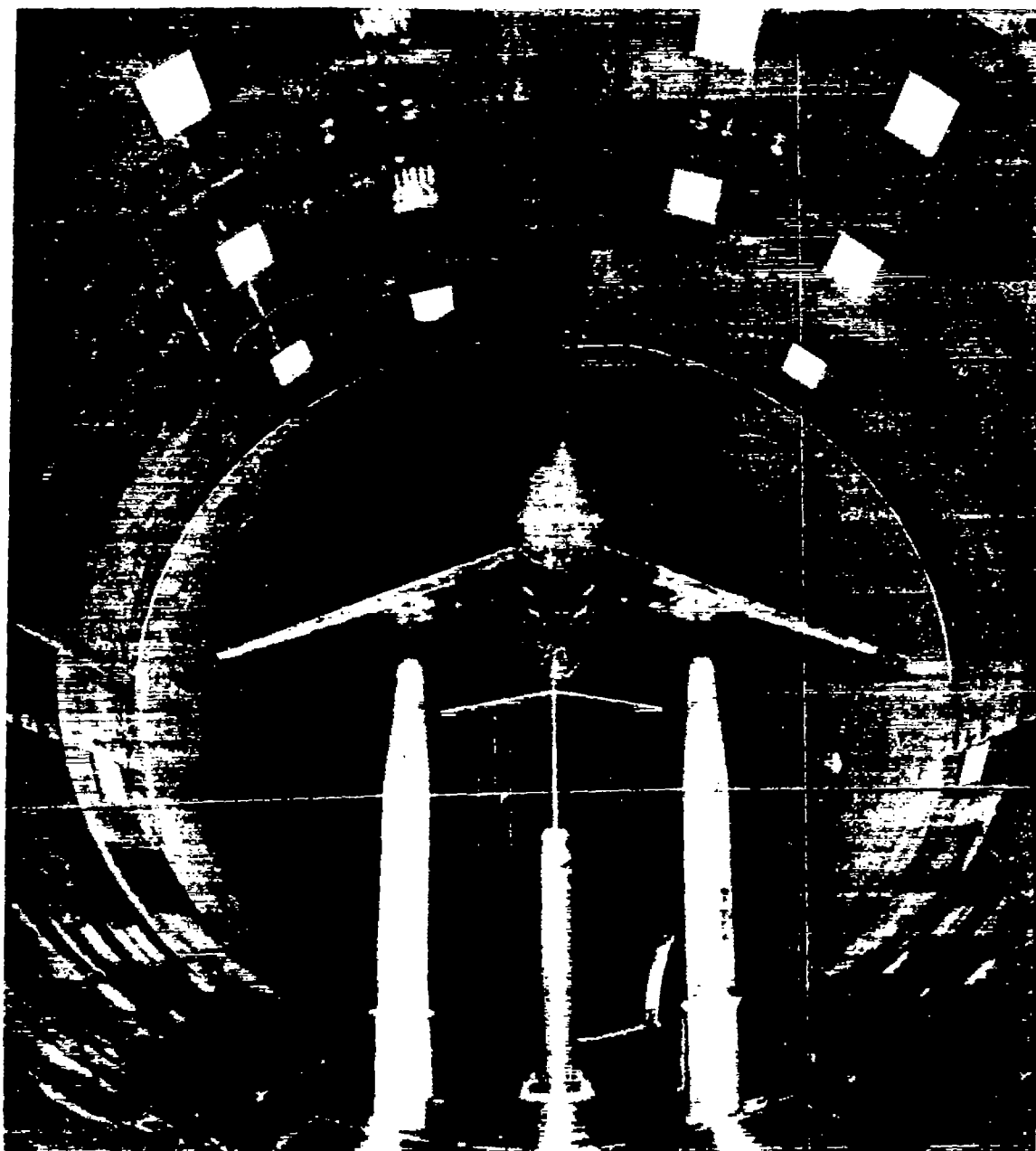


Figure 2.- Details and locations of the leading-edge and trailing-edge flaps. All dimensions are in inches.



L-60308

Figure 3.- The 47.7° sweptback wing-fuselage combination of aspect ratio 6.0 mounted in the Langley 19-foot pressure tunnel with the tail in the low position.

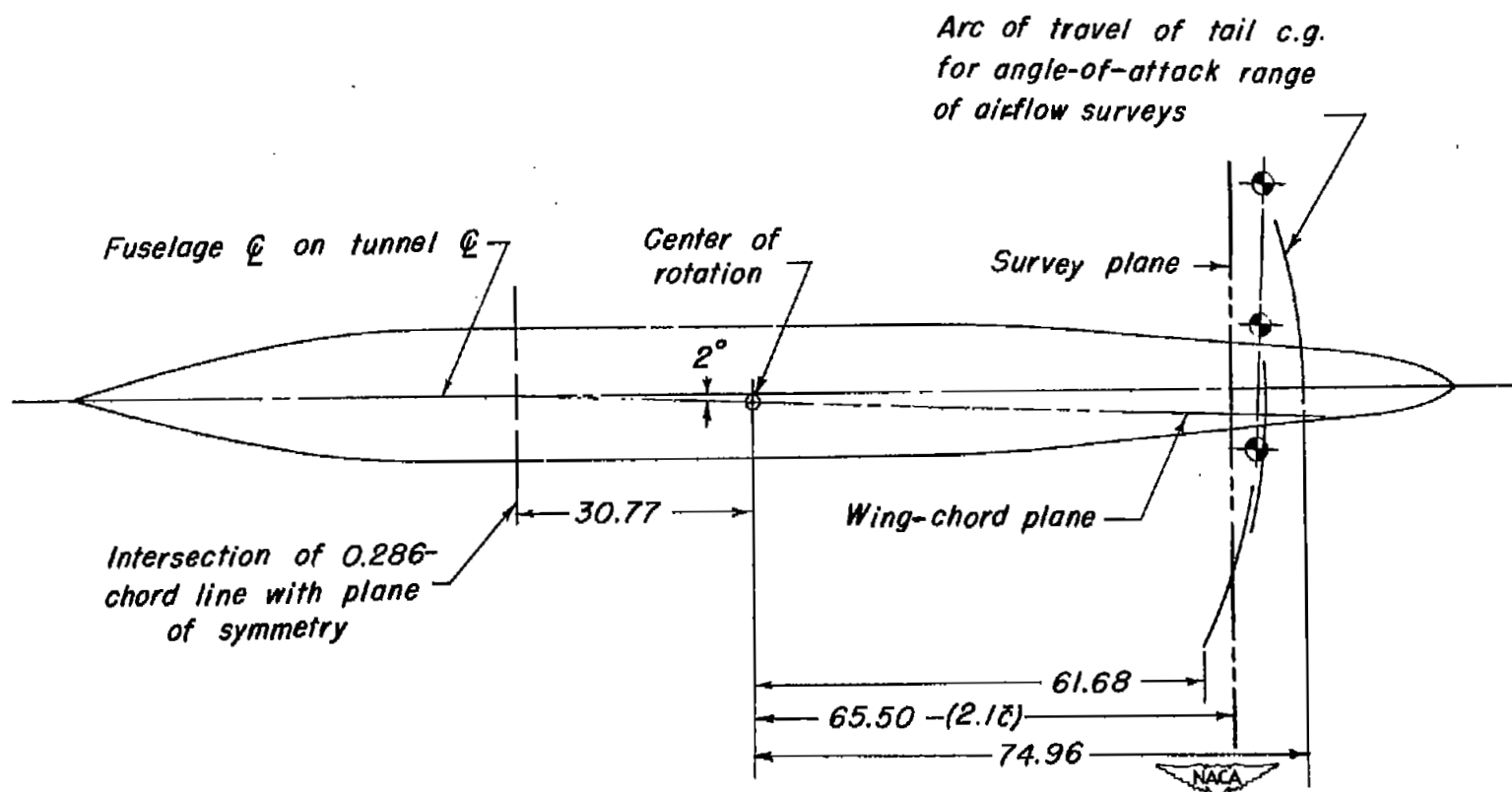


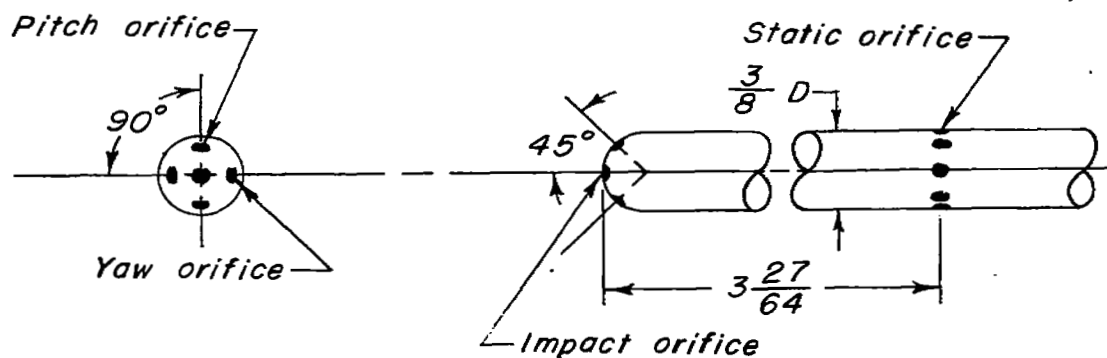
Figure 4.- Location of air-stream-survey plane. All dimensions are in inches.



(a) Photograph of rake head.

NACA

L-47123.1



(b) Sketch of tube head.

Figure 5.- Air-stream-survey rake used in Langley 19-foot pressure tunnel.
All dimensions are in inches.

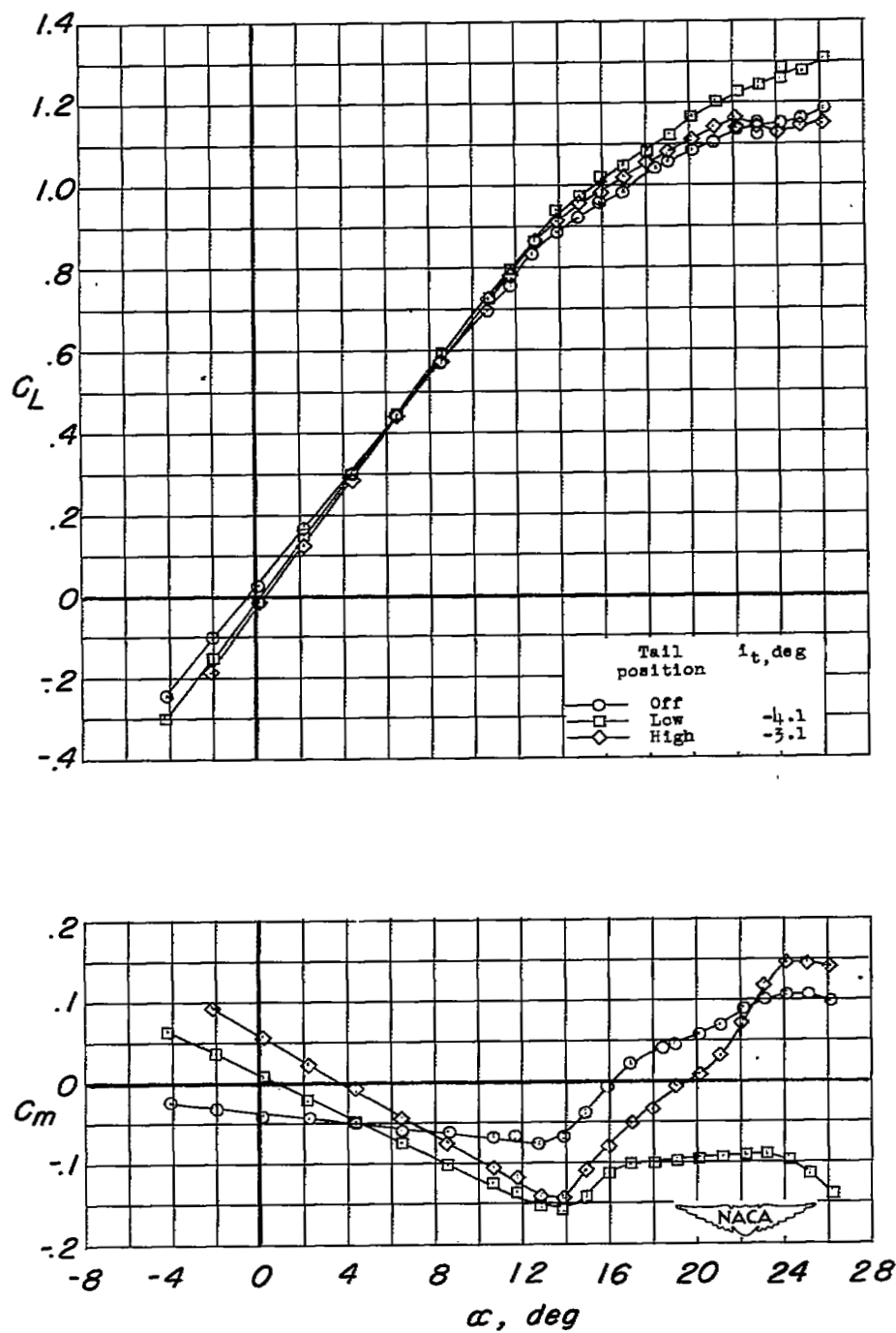
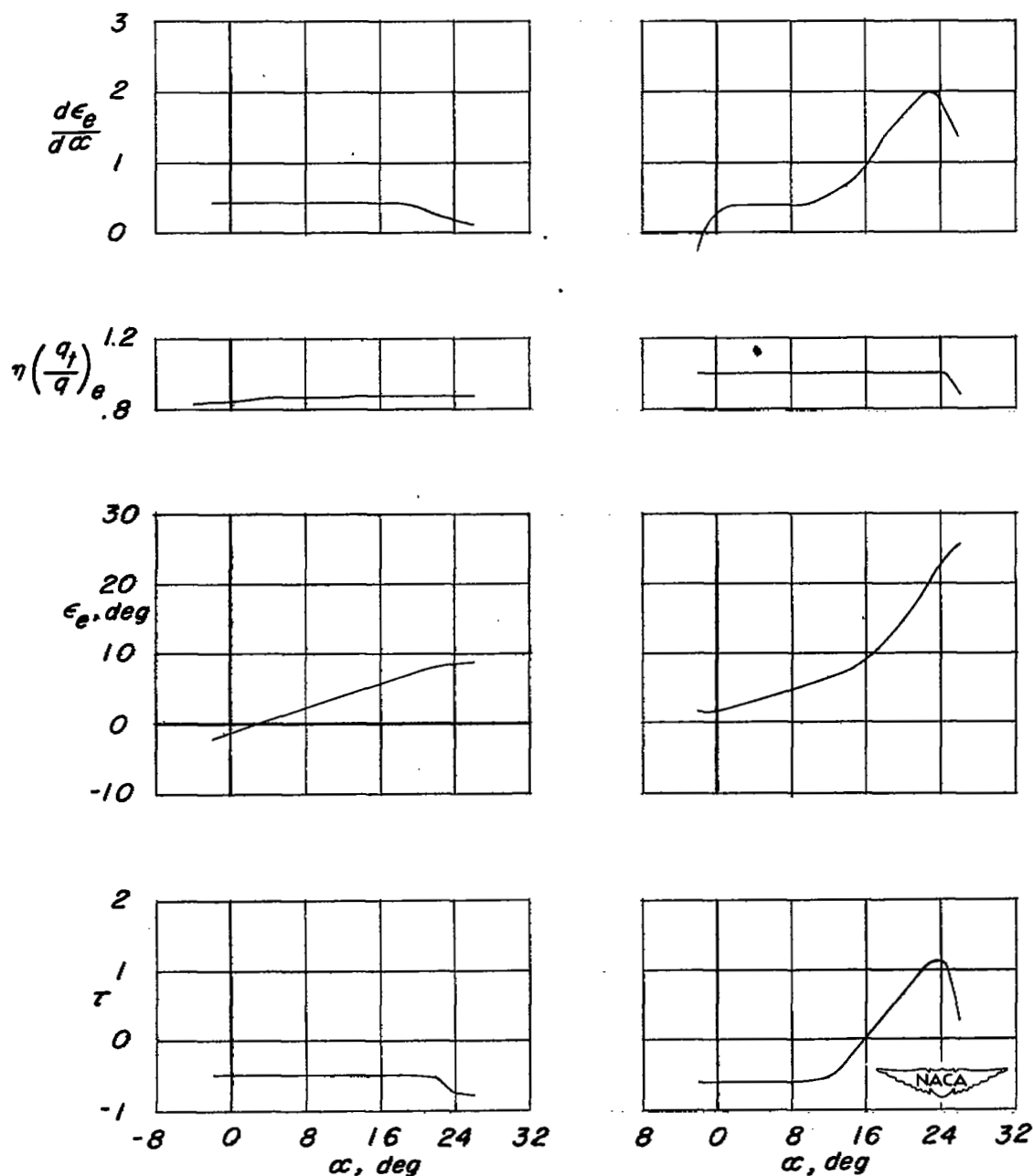


Figure 6.- Effects of horizontal-tail position on the variation of C_L and C_m with α for a 47.7° sweptback wing-fuselage combination of aspect ratio 5.1. Flaps neutral; $R = 6.0 \times 10^6$.



(a) Low tail.

(b) High tail.

Figure 7.- Variation with angle of attack of the tail effectiveness parameter, effective downwash angle, dynamic-pressure ratio and rate of change of downwash angle with angle of attack for the high and low tail positions on the 47.7° sweptback wing-fuselage combination of aspect ratio 5.1. Flaps neutral; $R = 6.0 \times 10^6$.

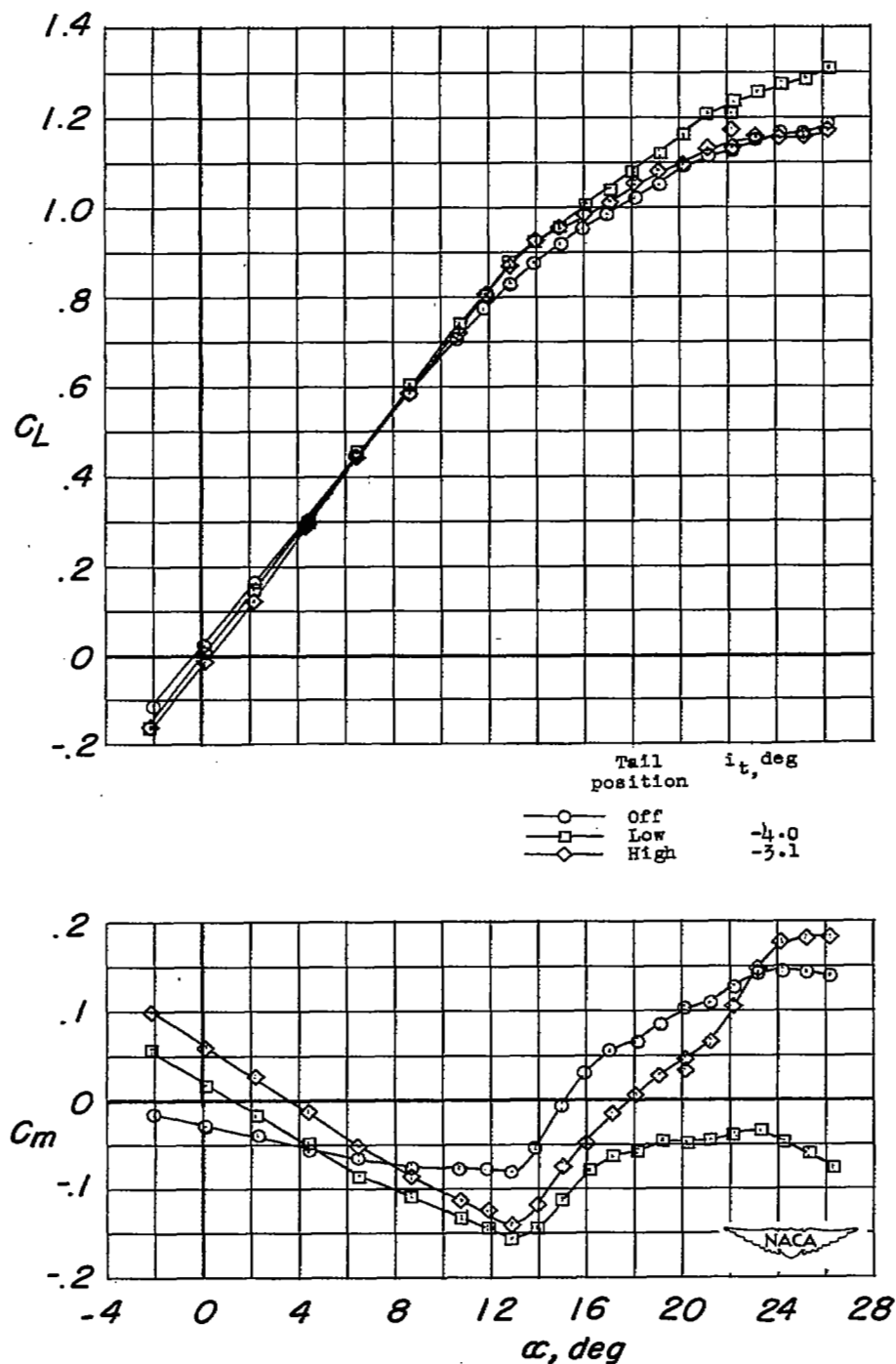
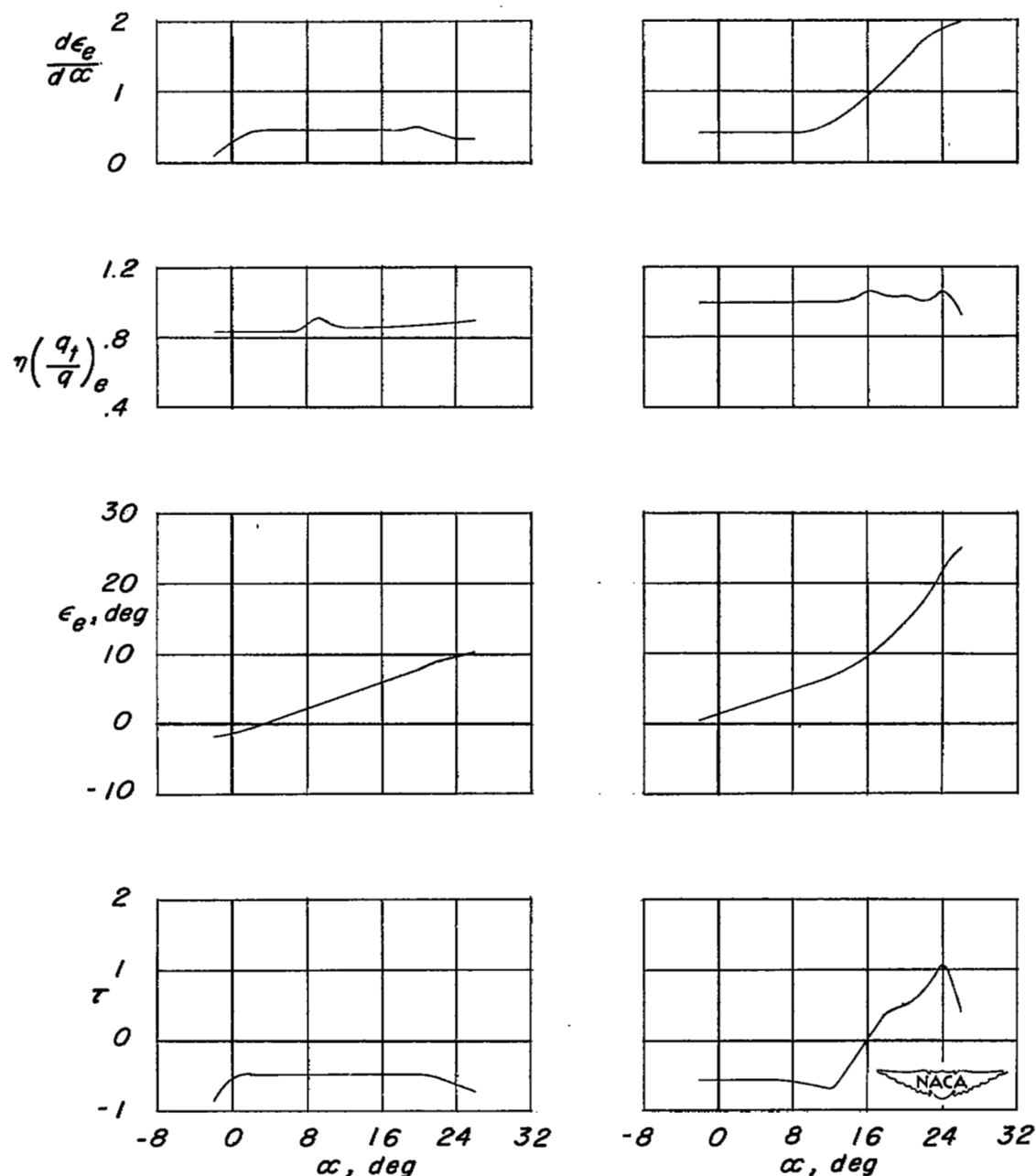


Figure 8.- Effects of horizontal-tail position on the variation of C_L and C_m with α for a 47.7° sweptback wing-fuselage combination of aspect ratio 6.0. Flaps neutral; $R = 6.0 \times 10^6$.



(a) Low tail.

(b) High tail.

Figure 9.- Variation with angle of attack of the tail effectiveness parameter, effective downwash angle, dynamic-pressure ratio and rate of change of downwash angle with angle of attack for the high and low tail positions on the 47.7° sweptback wing-fuselage combination of aspect ratio 6.0. Flaps neutral; $R = 6.0 \times 10^6$.

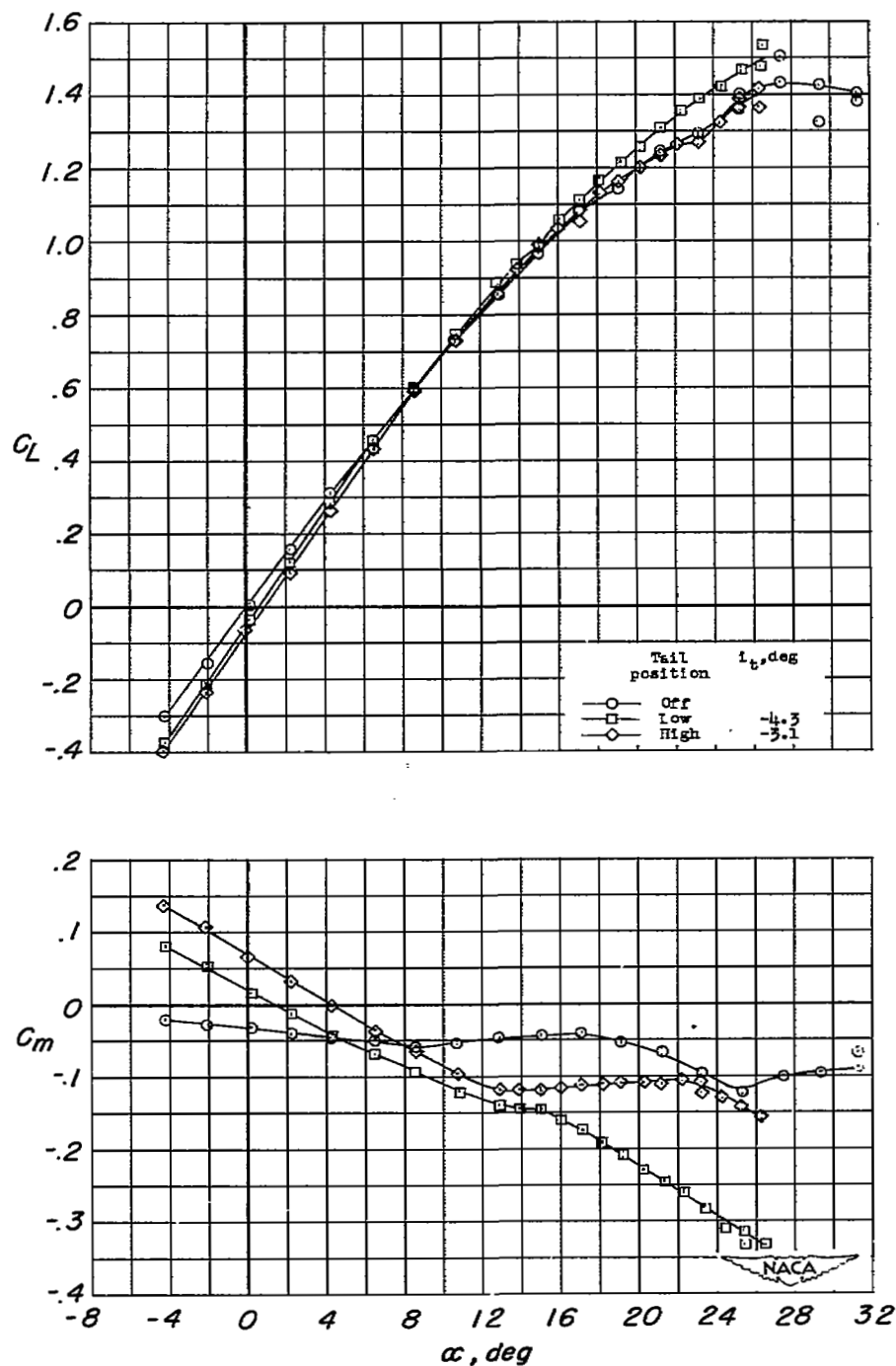
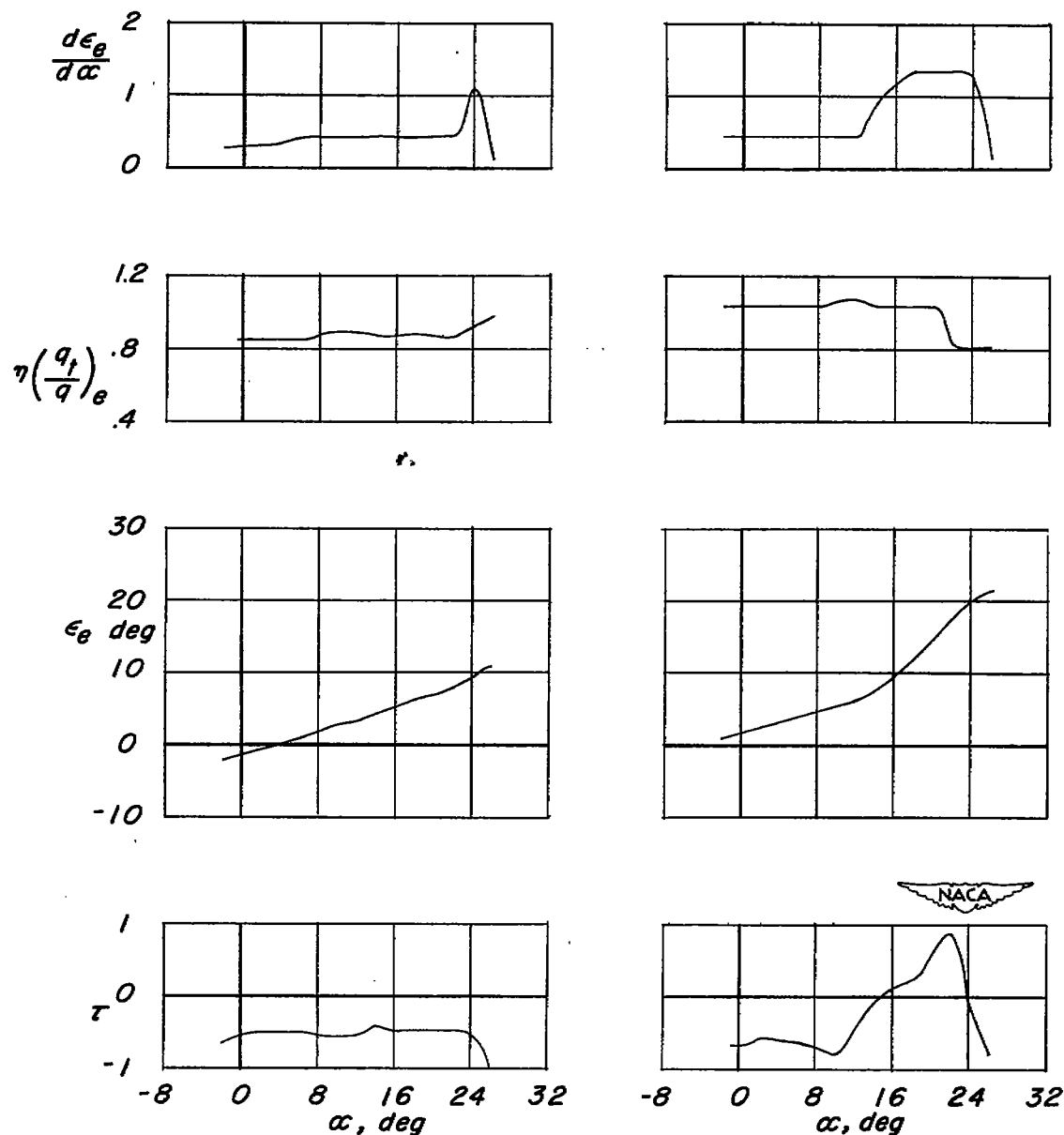


Figure 10.- Effects of horizontal-tail position on the variation of C_L and C_m with α for a 47.7° sweptback wing-fuselage combination of aspect ratio 5.1. $0.475b/2$ leading-edge flaps deflected; $R = 6.0 \times 10^6$.



(a) Low tail.

(b) High tail.

Figure 11.- Variation with angle of attack of the tail effectiveness parameter, effective downwash angle, dynamic-pressure ratio and rate of change of downwash angle with angle of attack for the high and low tail positions on the 47.7° sweptback wing-fuselage combination of aspect ratio 5.1. $0.475b/2$ leading-edge flaps deflected; $R = 6.0 \times 10^6$.

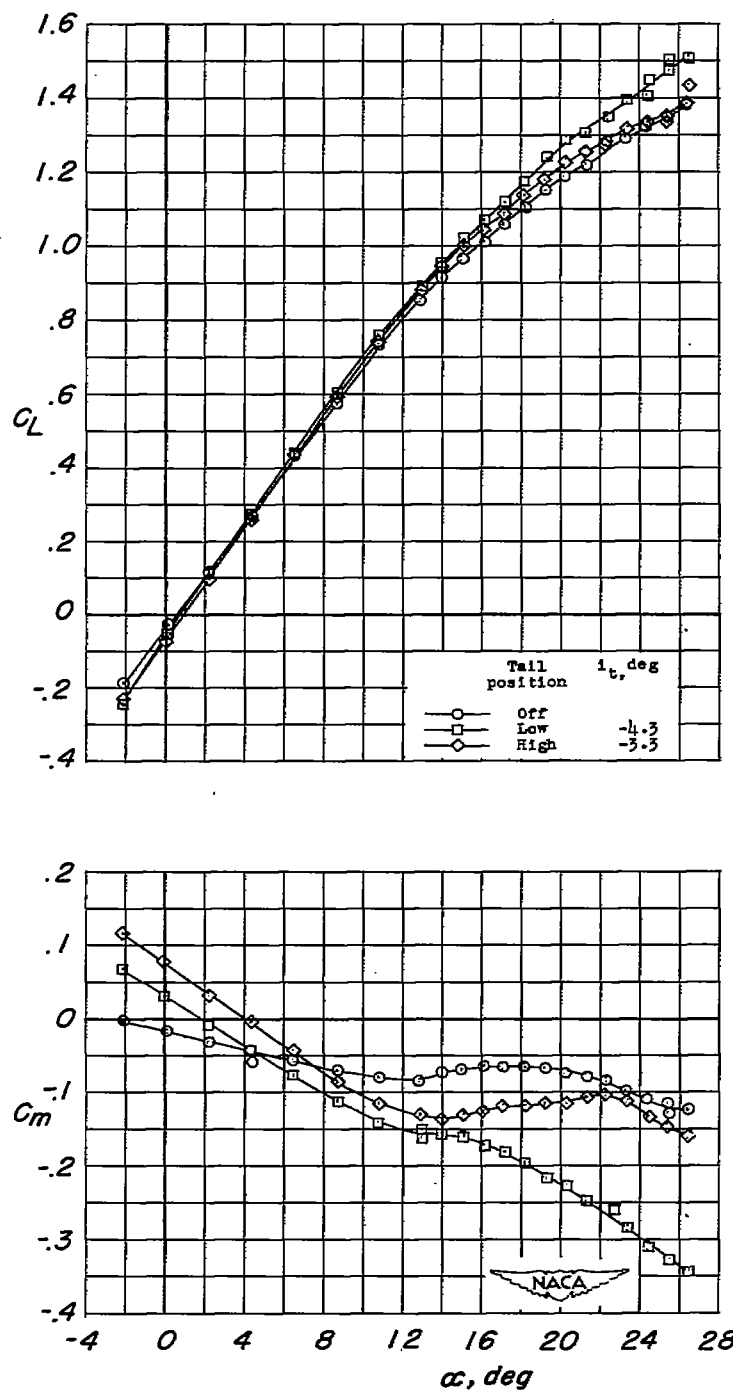
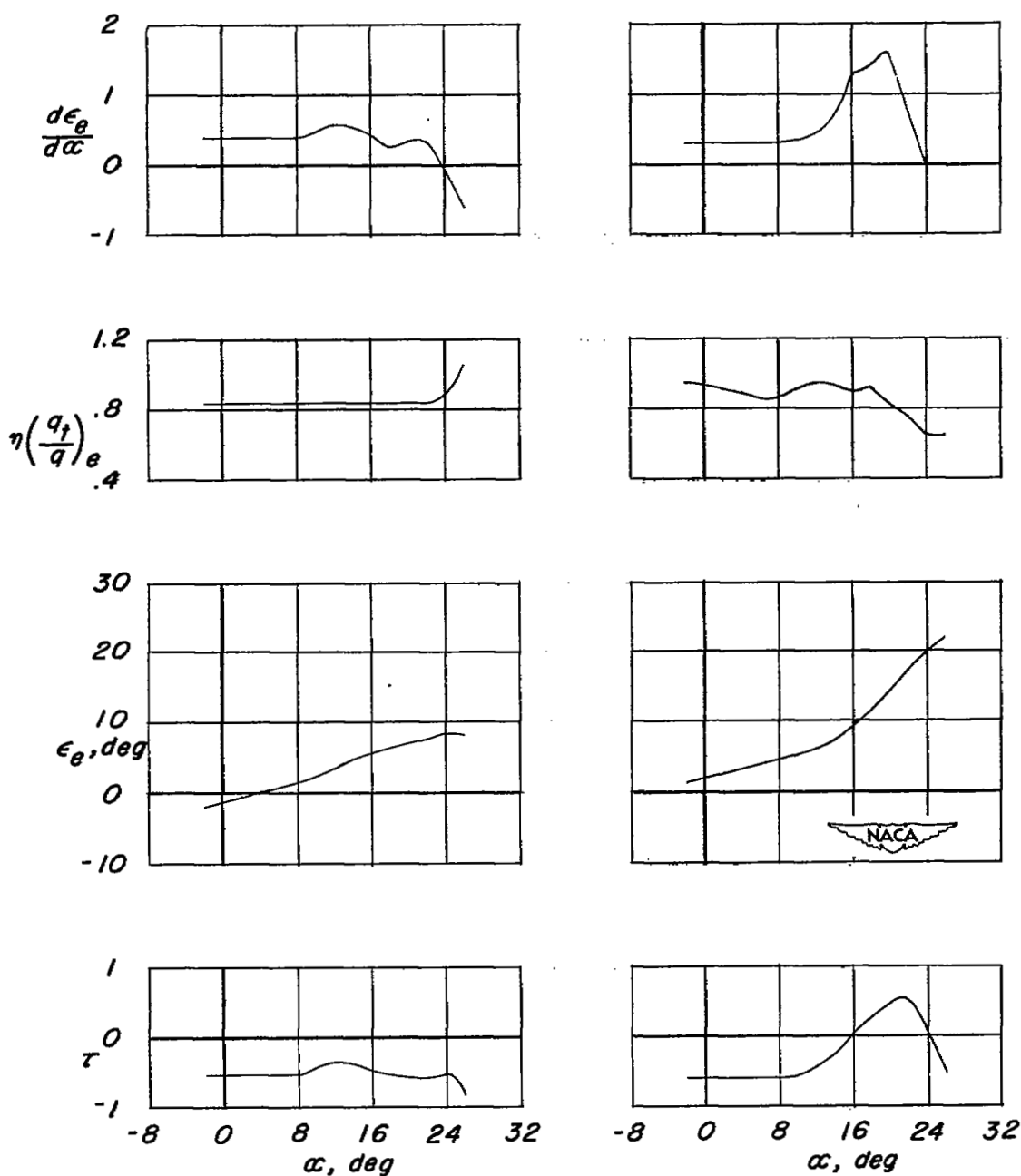


Figure 12.- Effects of horizontal-tail position on the variation of C_L and C_m with α for a 47.7° sweptback wing-fuselage combination of aspect ratio 6.0. 0.48lb/2 leading-edge flaps deflected; $R = 6.0 \times 10^6$.



(a) Low tail.

(b) High tail.

Figure 13.- Variation with angle of attack of the tail effectiveness parameter, effective downwash angle, dynamic-pressure ratio and rate of change of downwash angle with angle of attack for the high and low tail positions on the 47.7° sweptback wing-fuselage combination of aspect ratio 6.0. 0.48lb/2 leading-edge flaps deflected; $R = 6.0 \times 10^6$.

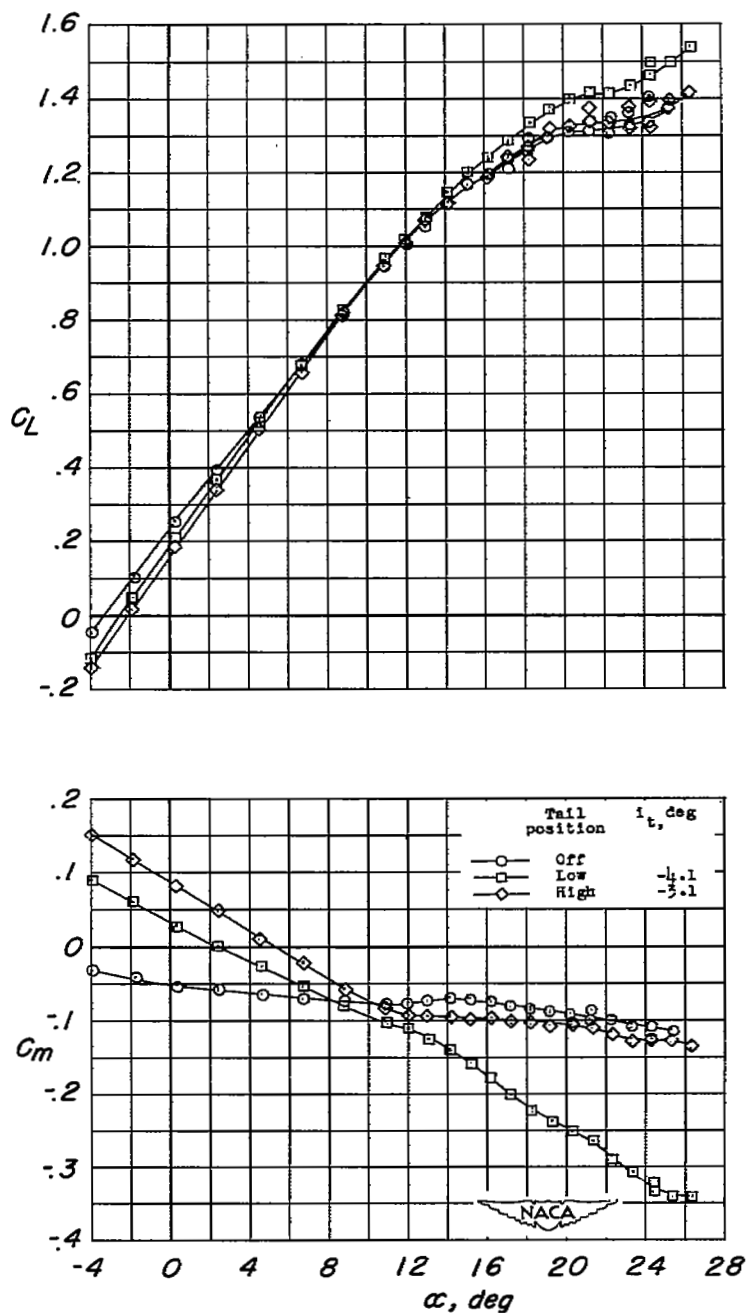
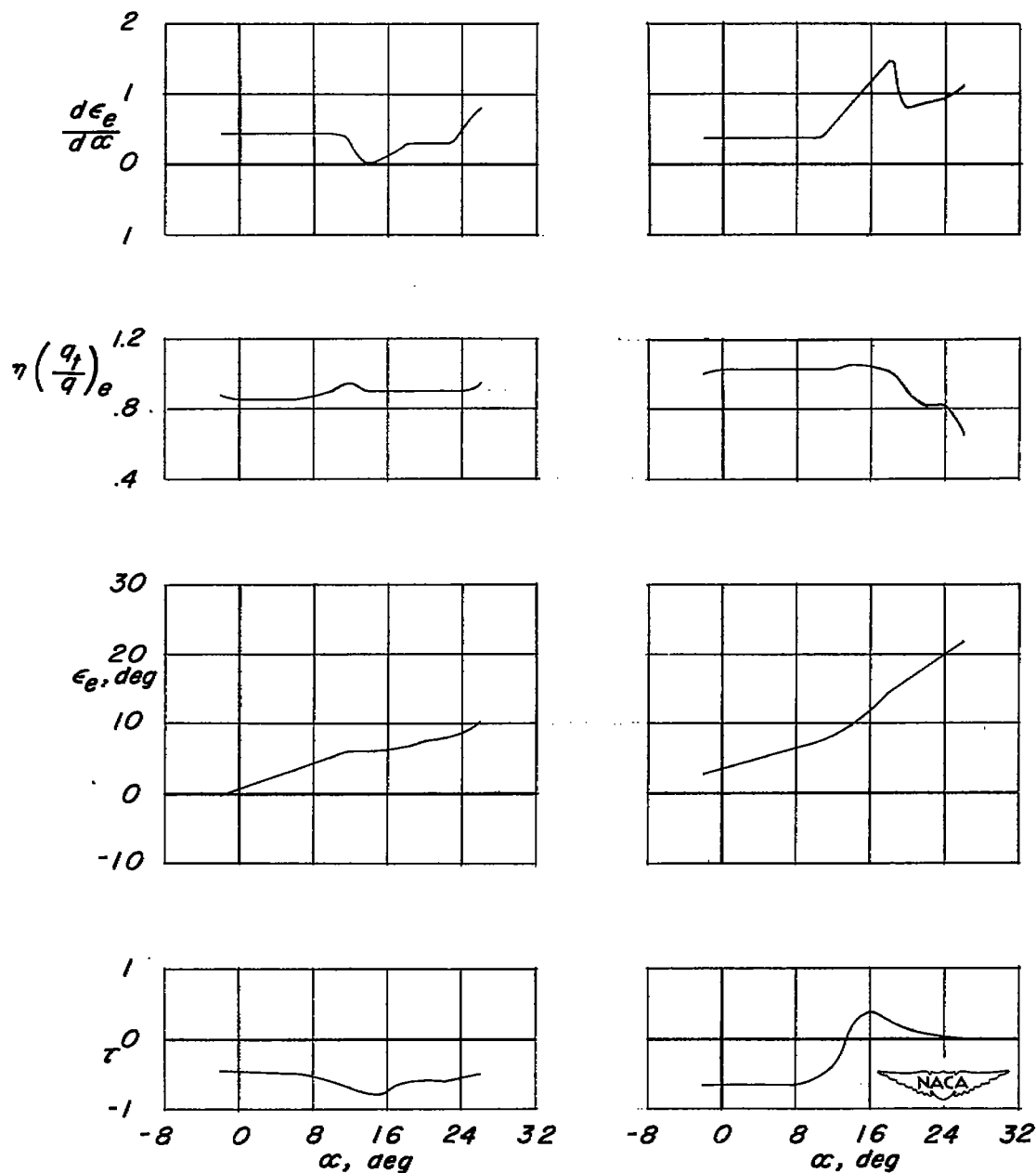


Figure 14.- Effects of horizontal-tail position on the variation of C_L and C_m with α for a 47.7° sweptback wing-fuselage combination of aspect ratio 5.1. $0.400b/2$ split flaps and $0.475b/2$ leading-edge flaps; $R = 6.0 \times 10^6$.



(a) Low tail.

(b) High tail.

Figure 15.- Variation with angle of attack of the tail effectiveness parameter, effective downwash angle, dynamic-pressure ratio and rate of change of downwash angle with angle of attack for the high and low tail positions on the 47.7° sweptback wing-fuselage combination of aspect ratio 5.1. 0.400b/2 split flaps and 0.475b/2 leading-edge flaps; $R = 6.0 \times 10^6$.

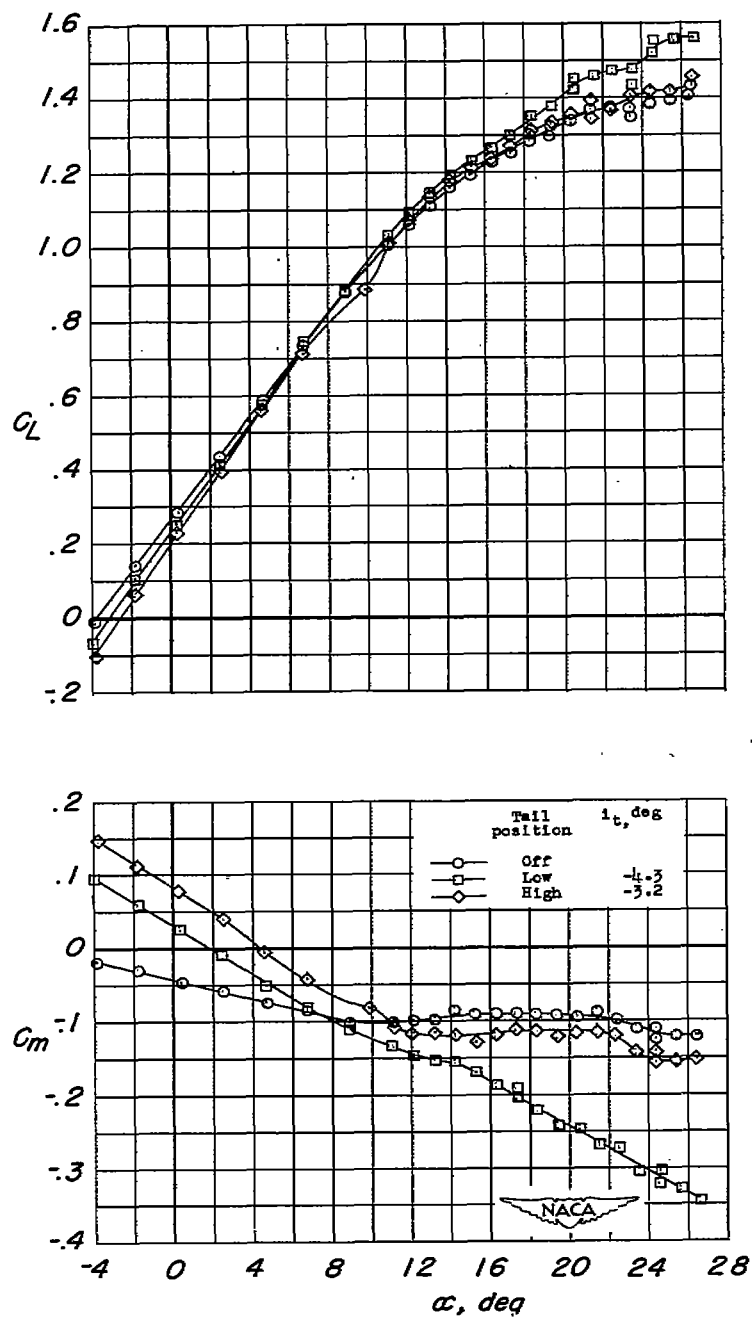
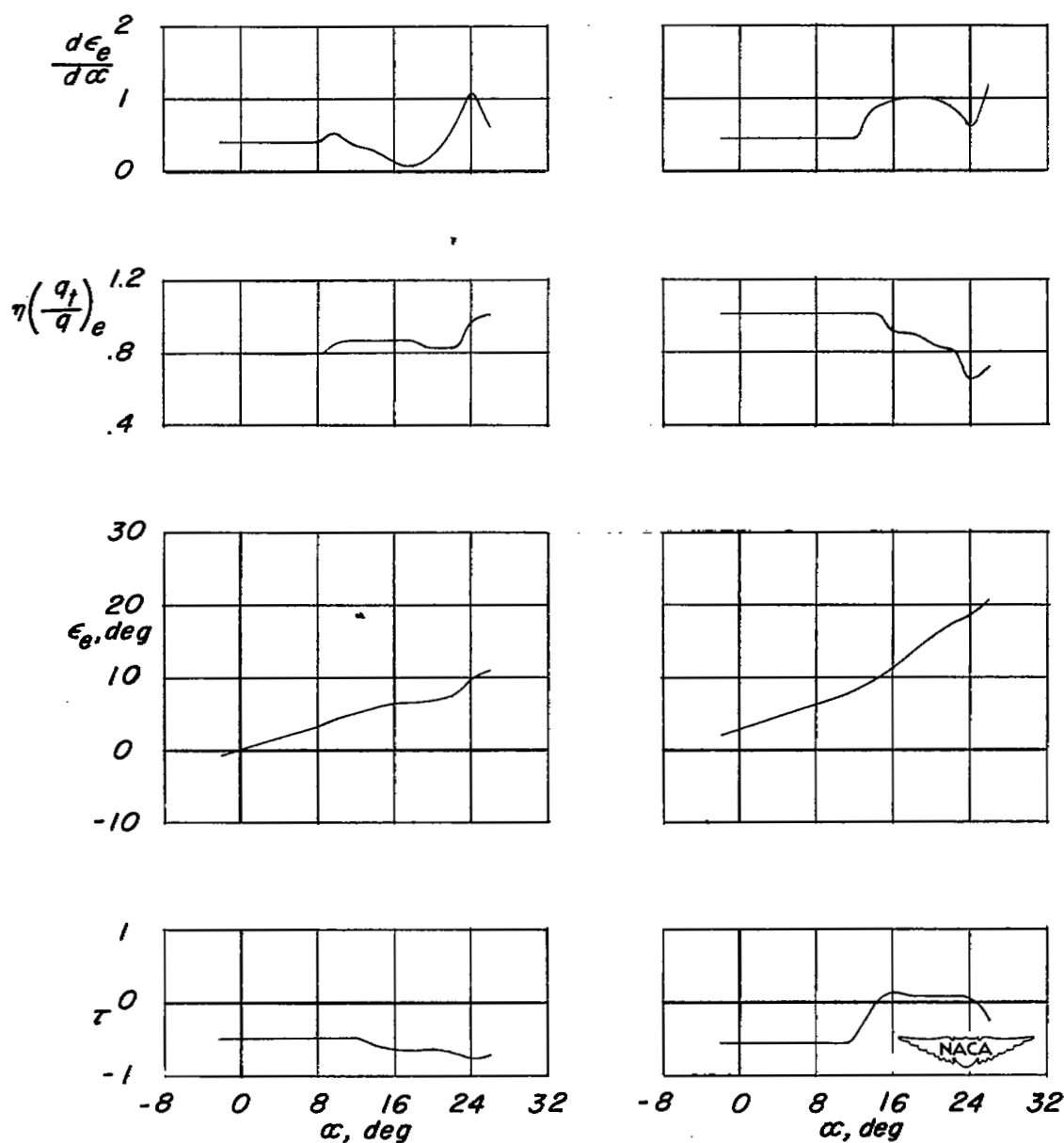


Figure 16.- Effects of horizontal-tail position on the variation of C_L and C_m with α for a 47.7° sweptback wing-fuselage combination of aspect ratio 6.0. $0.449b/2$ split flaps and $0.481b/2$ leading-edge flaps; $R = 6.0 \times 10^6$.



(a) Low tail.

(b) High tail.

Figure 17.- Variation with angle of attack of the tail effectiveness parameter, effective downwash angle, dynamic-pressure ratio and rate of change of downwash angle with angle of attack for the high and low tail positions on the 47.7° sweptback wing-fuselage combination of aspect ratio 6.0. 0.449b/2 split flaps and 0.481b/2 leading-edge flaps; $R = 6.0 \times 10^6$.

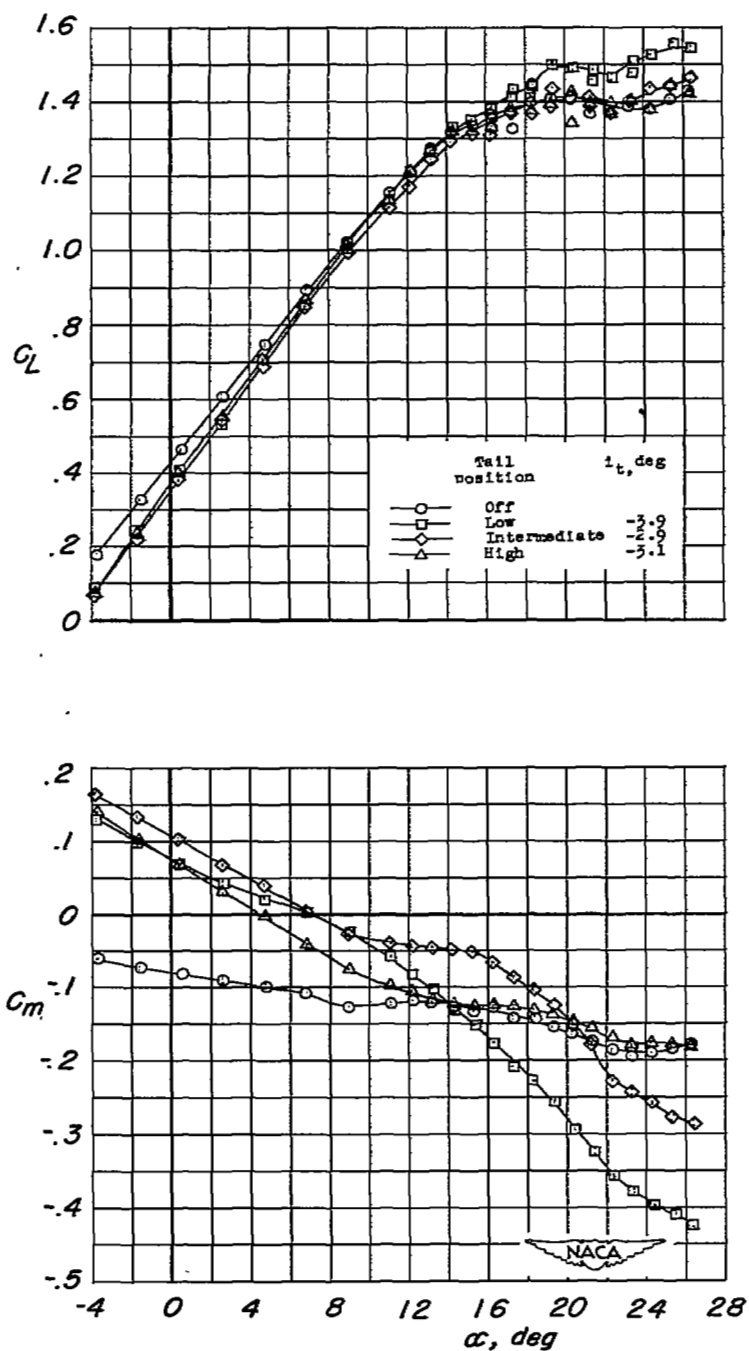
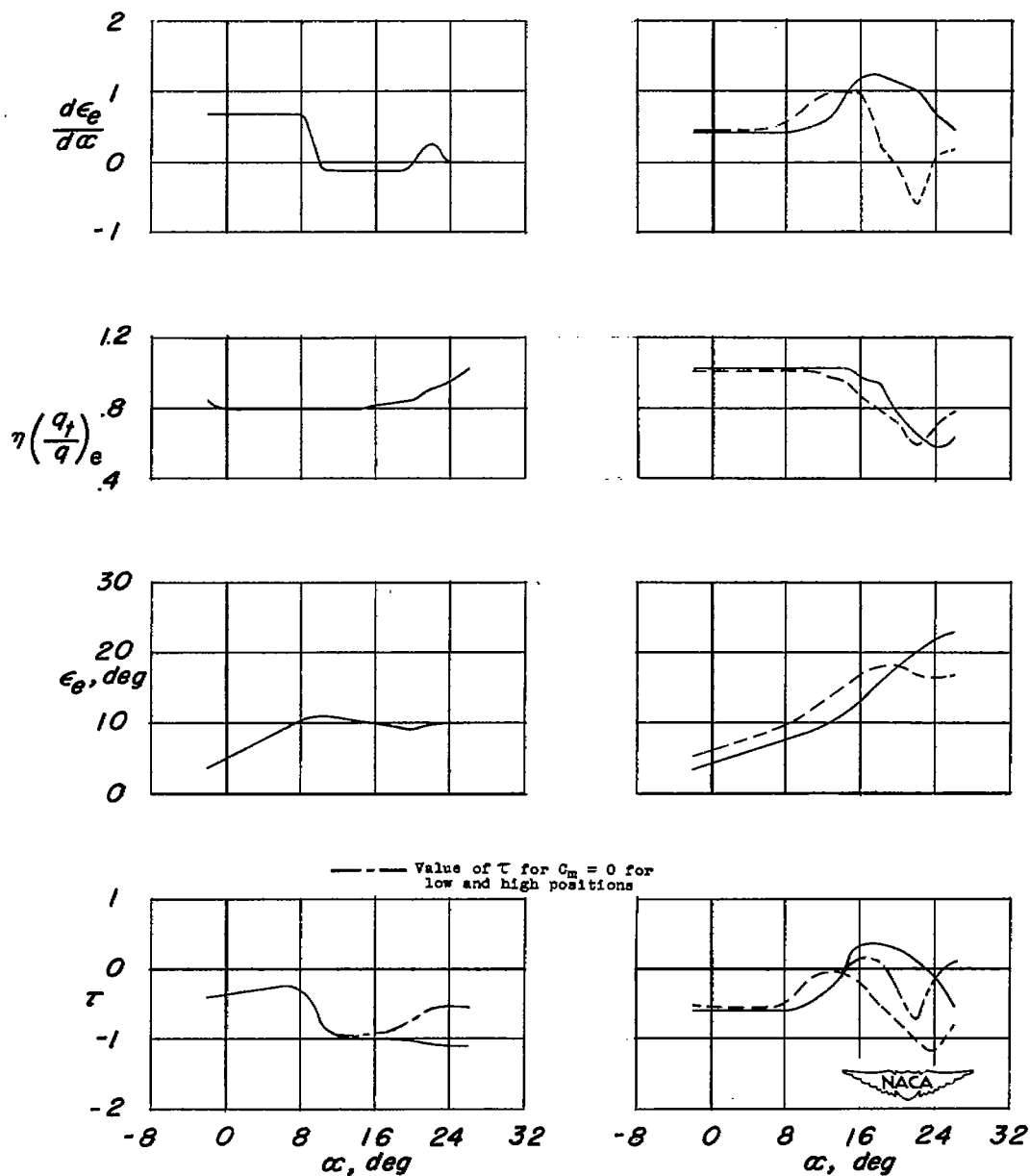


Figure 18.- Effects of horizontal-tail position on the variation of C_L and C_m with α for a 47.7° sweptback wing-fuselage combination of aspect ratio 5.1. $0.400b/2$ double slotted flaps and $0.475b/2$ leading-edge flaps; $R = 6.0 \times 10^6$.



(a) Low tail.

(b) High tail (solid curve) and intermediate tail (dashed curve).

Figure 19.- Variation with angle of attack of the tail effectiveness parameter, effective downwash angle, dynamic-pressure ratio and rate of change of downwash angle with angle of attack for the high, low, and intermediate tail positions on the 47.7° sweptback wing-fuselage combination of aspect ratio 5.1. $0.400b/2$ double slotted flaps and $0.475b/2$ leading-edge flaps; $R = 6.0 \times 10^6$.

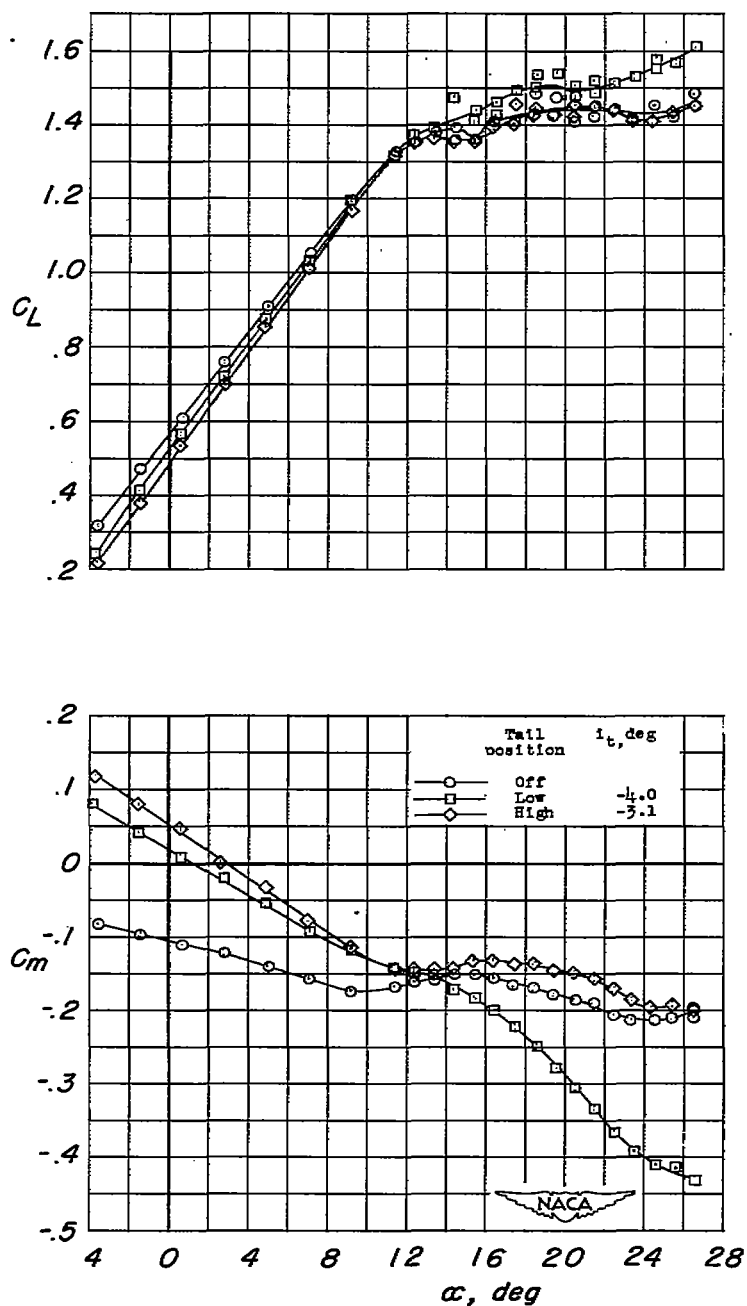
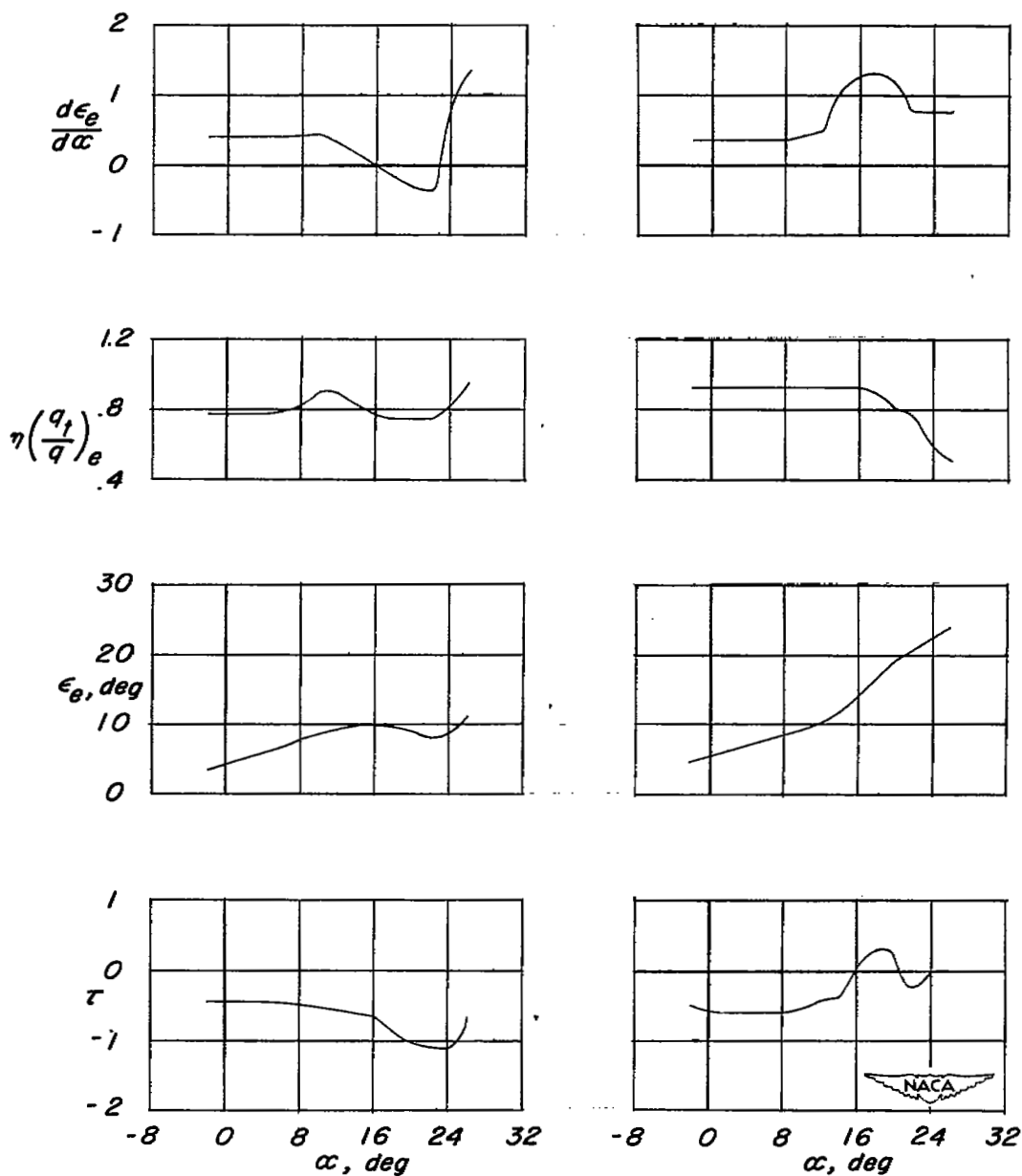


Figure 20.- Effects of horizontal-tail position on the variation of C_L and C_m with α for a 47.7° sweptback wing-fuselage combination of aspect ratio 6.0. 0.462b/2 double slotted flaps and 0.481b/2 leading-edge flaps; $R = 6.0 \times 10^6$.



(a) Low tail.

(b) High tail.

Figure 21.- Variation with angle of attack of the tail effectiveness parameter, effective downwash angle, dynamic-pressure ratio and rate of change of downwash angle with angle of attack for the high and low tail positions on the 47.7° sweptback wing-fuselage combination of aspect ratio 6.0. 0.462b/2 double slotted flaps and 0.481b/2 leading-edge flaps; $R = 6.0 \times 10^6$.

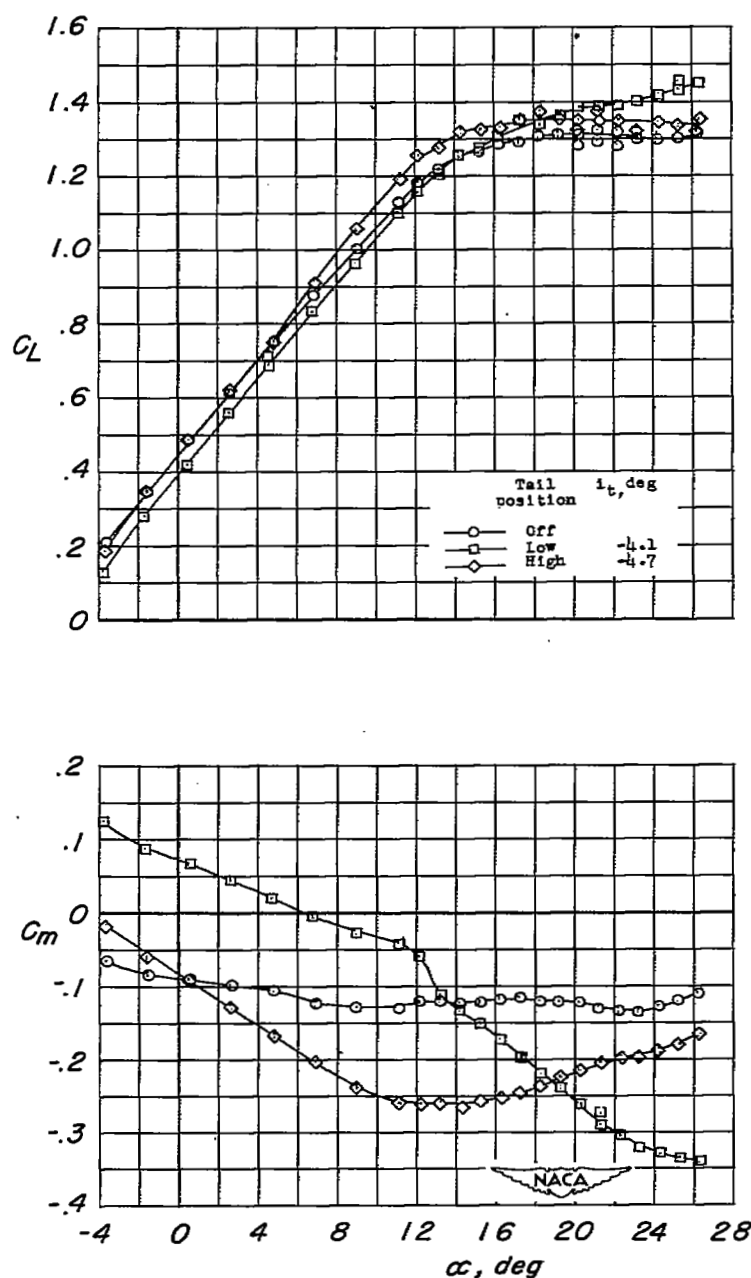
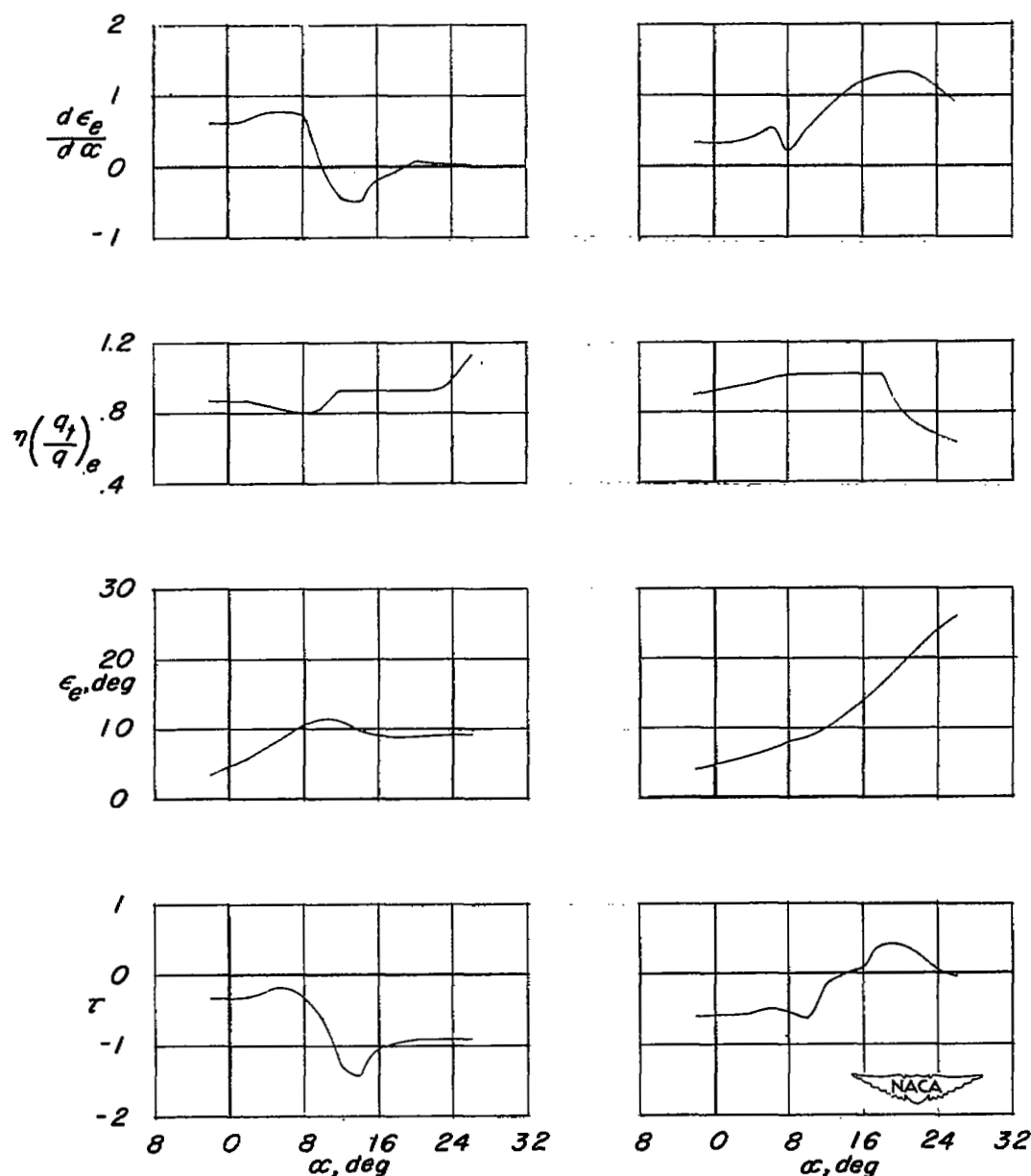


Figure 22.- Effects of horizontal-tail position on the variation of C_L and C_m with α for a 47.7° sweptback wing-fuselage combination of aspect ratio 5.1. $0.400b/2$ double slotted flaps and $0.375b/2$ drooped nose ($\delta_n = 20^\circ$); $R = 6.0 \times 10^6$.



(a) Low tail.

(b) High tail.

Figure 23.- Variation with angle of attack of the tail effectiveness parameter, effective downwash angle, dynamic-pressure ratio and rate of change of downwash angle with angle of attack for the high and low tail positions on the 47.7° sweptback wing-fuselage combination of aspect ratio 5.1. $0.400b/2$ double slotted flaps and $0.375b/2$ drooped nose ($\delta_n = 20^\circ$); $R = 6.0 \times 10^6$.

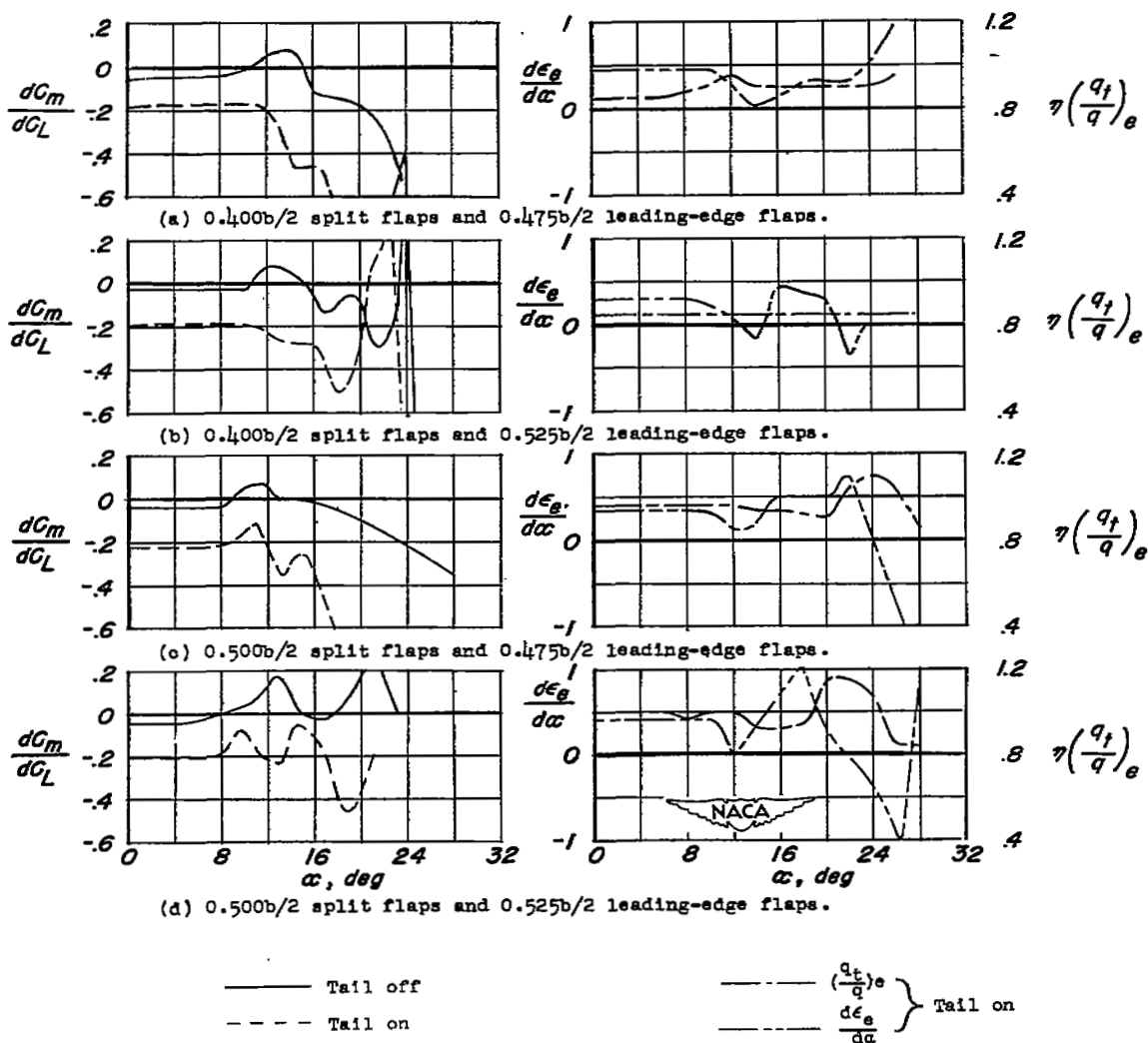
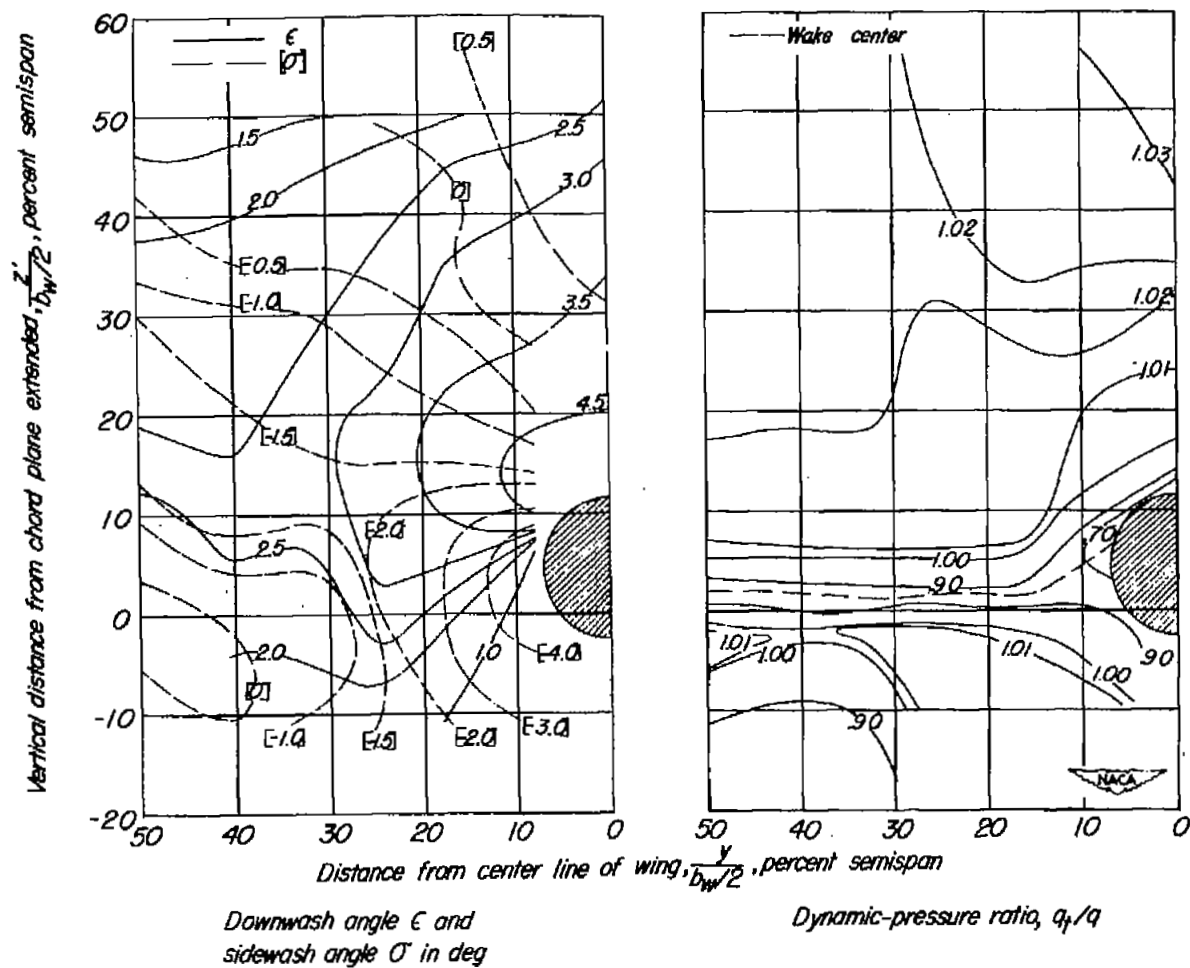


Figure 24.- Variation of dC_m/dC_L , $d\epsilon_e/d\alpha$ and $\eta(q_t/q_e)$ with angle of attack for various spans of leading-edge flaps and split flaps on the wing-fuselage combination of aspect ratio 5.1 with and without the tail in the low position. $R = 6.0 \times 10^6$.



(a) $\alpha = 4.4^\circ$.

Figure 25.- Contour charts of the air-flow characteristics in the region of the horizontal tail. Flaps neutral; aspect ratio, 5.1; $R = 6.0 \times 10^6$. Shaded areas indicate extrapolated data.

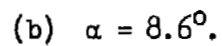
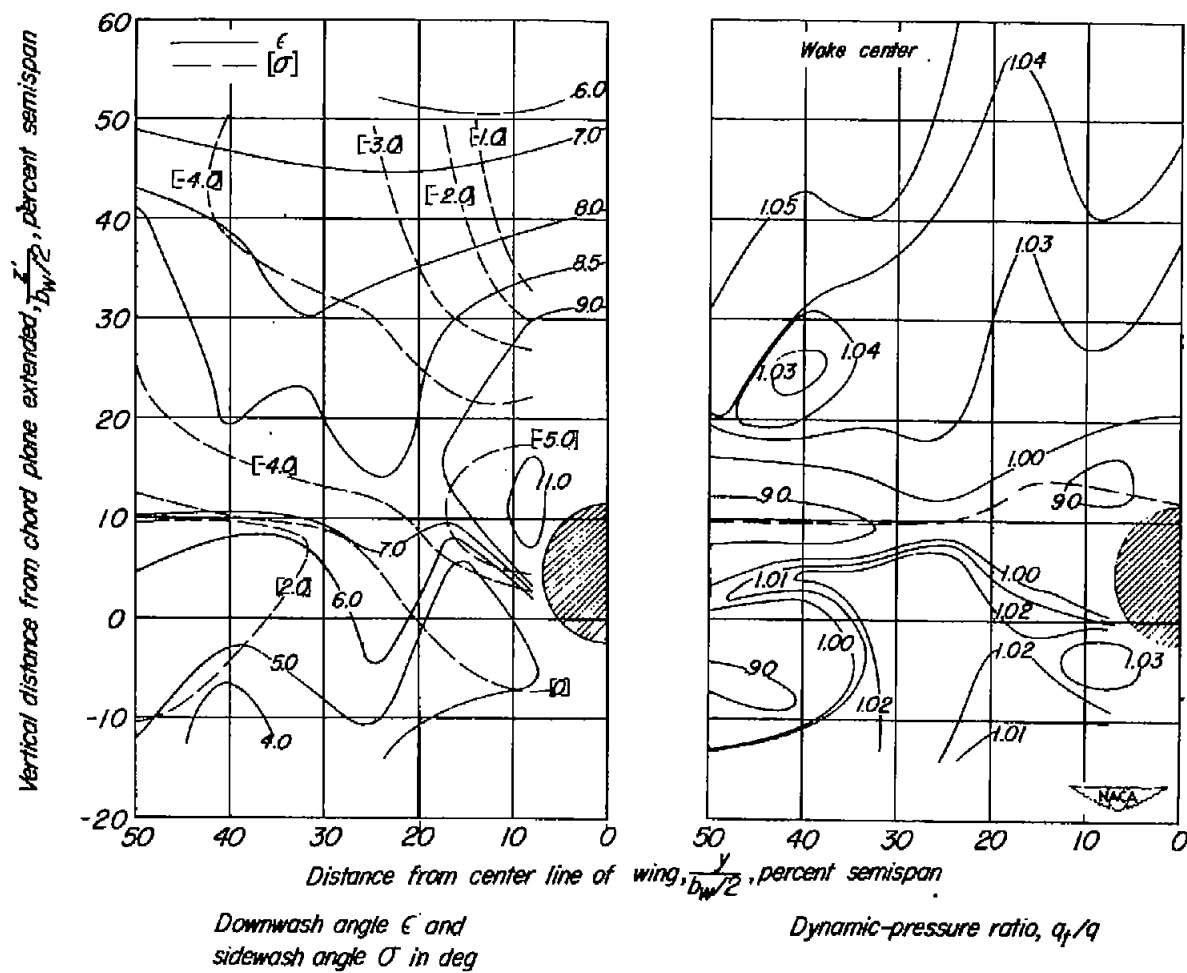
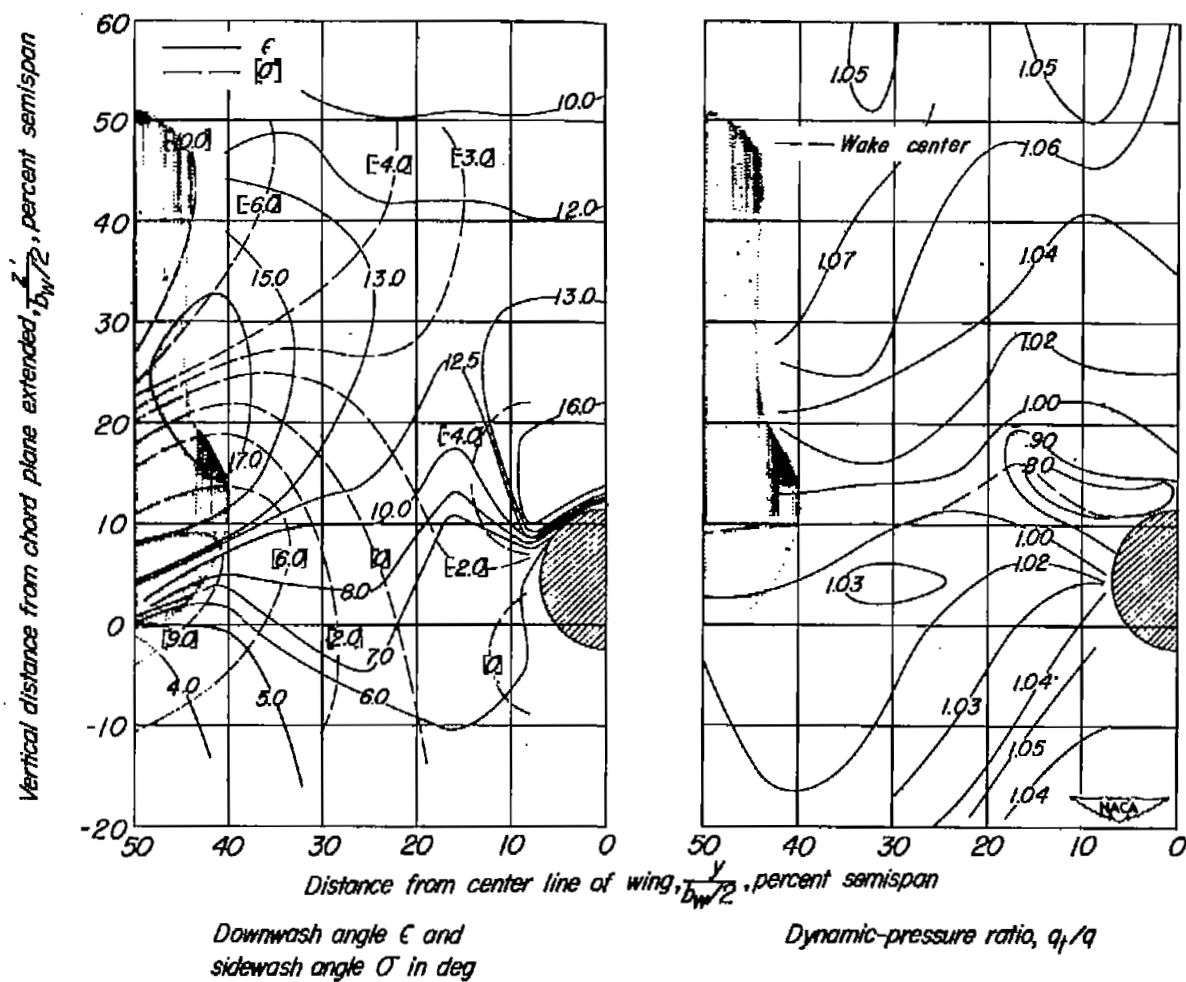


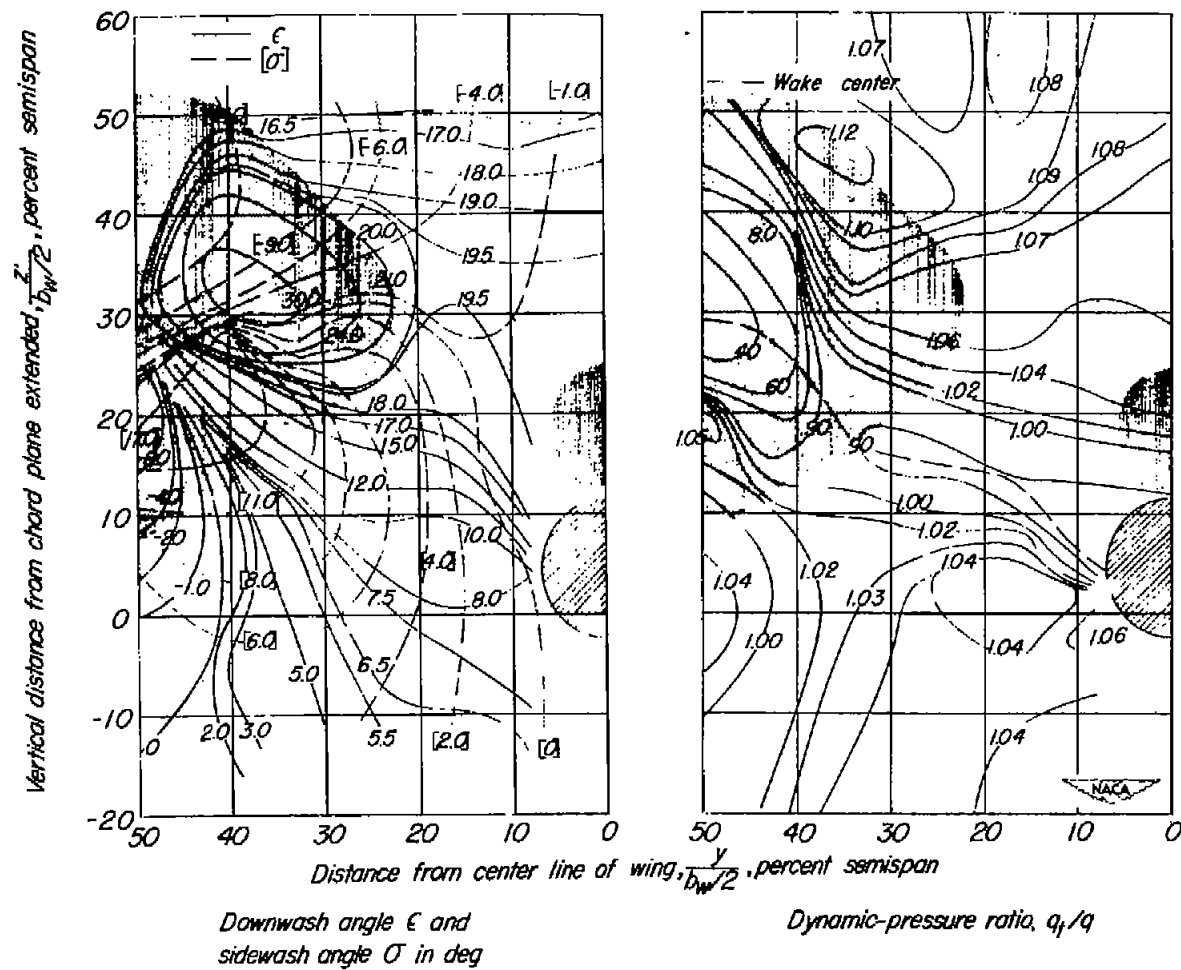
Figure 25.- Continued.





(d) $\alpha = 19.0^\circ$.

Figure 25.- Continued.



(e) $\alpha = 23.1^\circ$.

Figure 25.- Concluded.

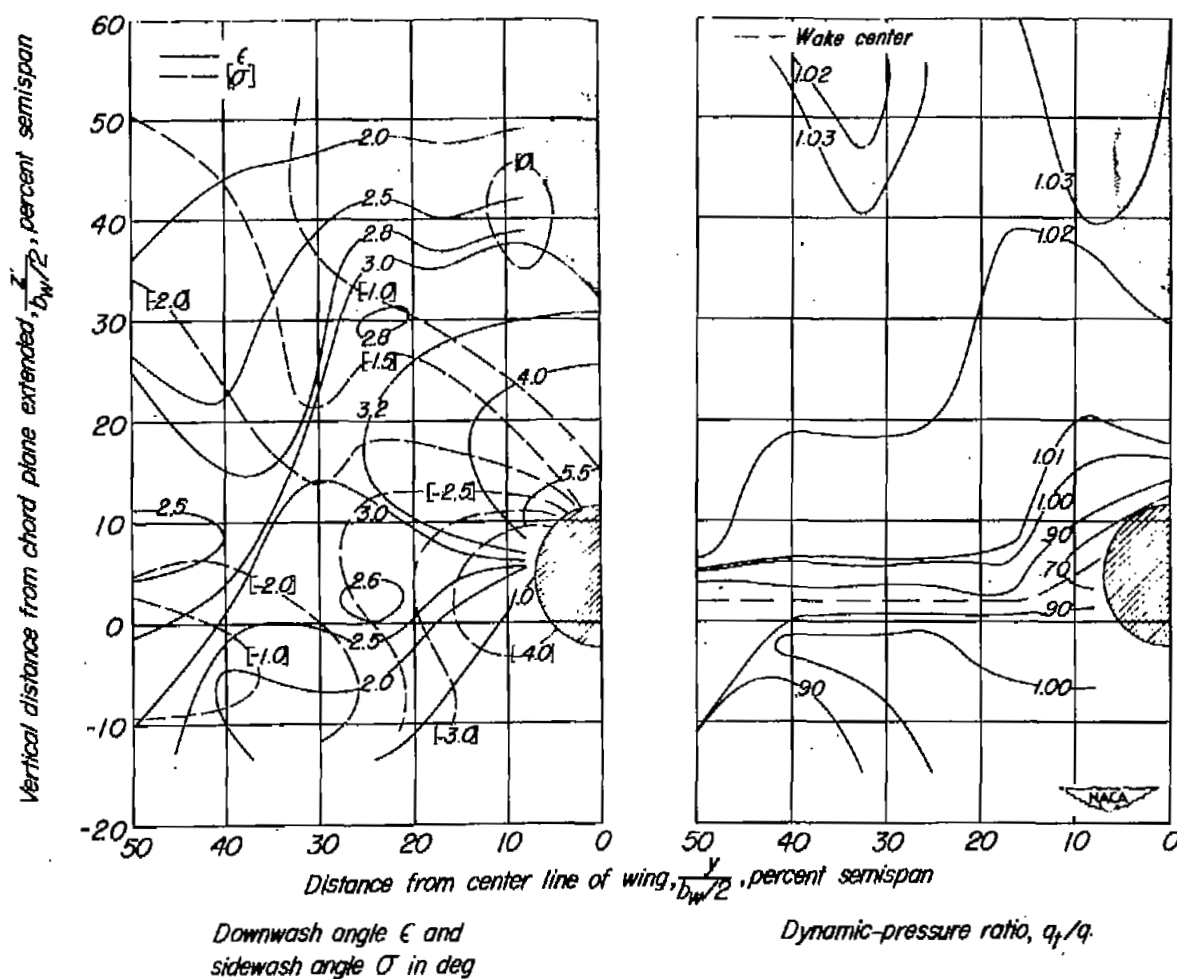
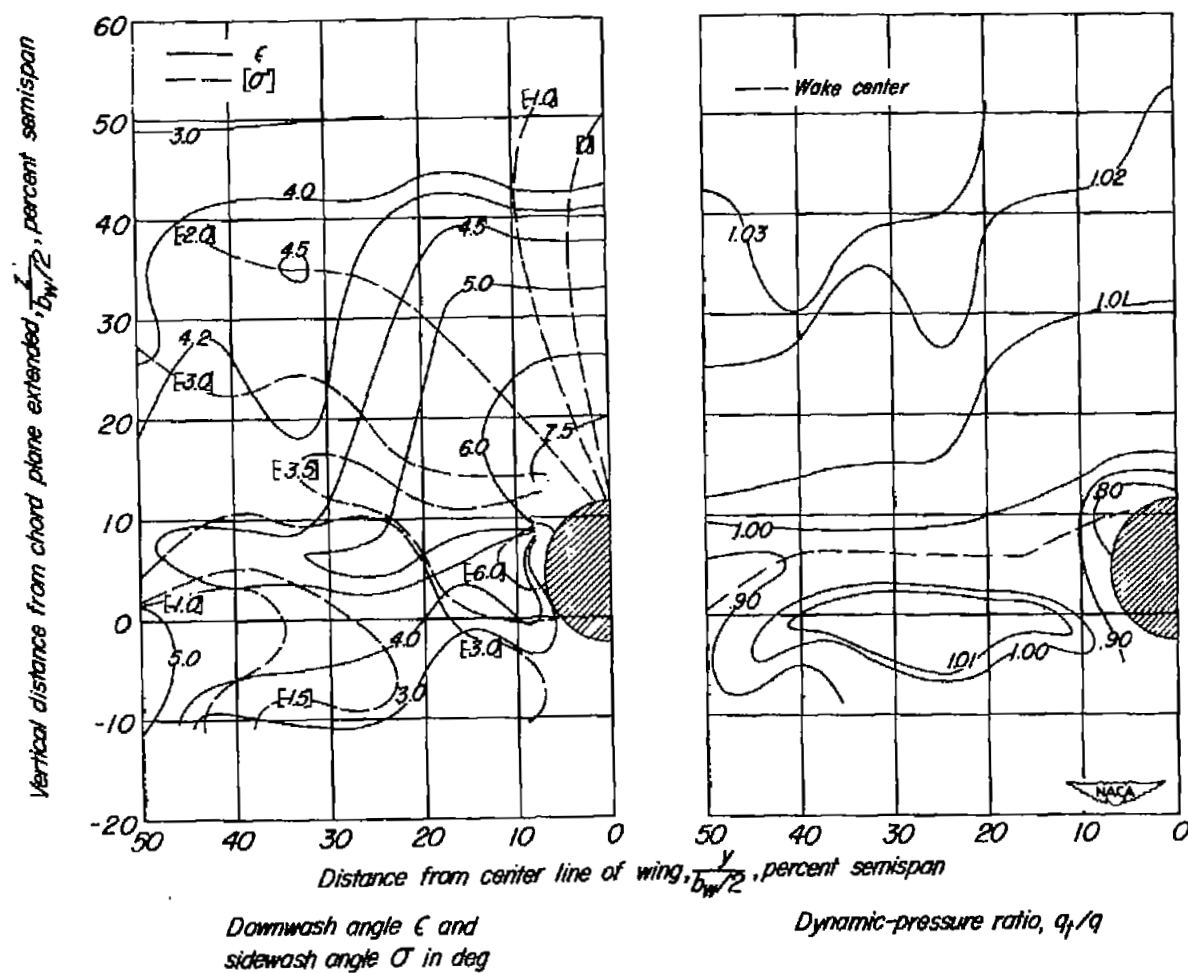
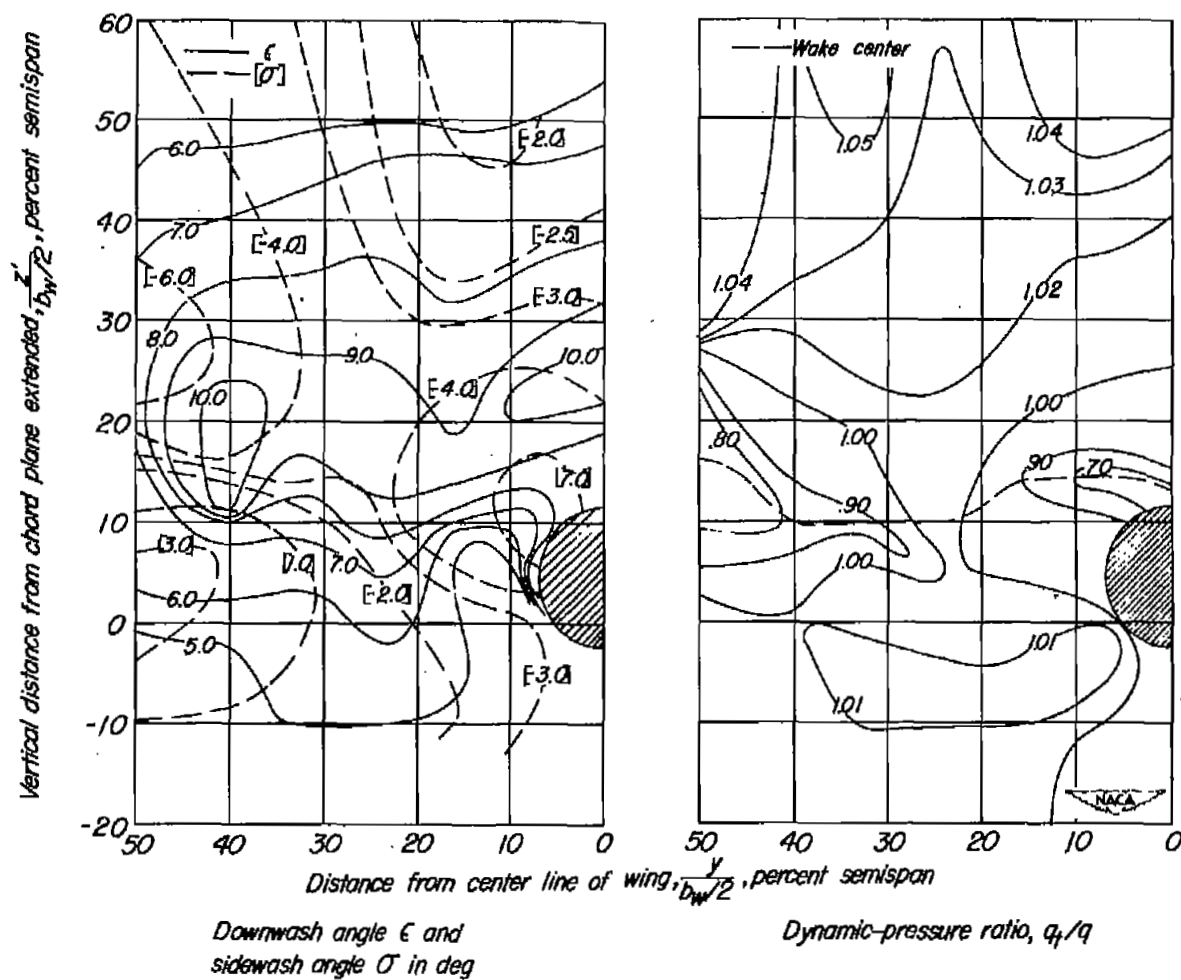


Figure 26.- Contour charts of the air-flow characteristics in the region of the horizontal tail. $0.475b/2$ leading-edge flaps deflected; aspect ratio, 5.1; $R = 6.0 \times 10^6$. Shaded areas indicate extrapolated data.



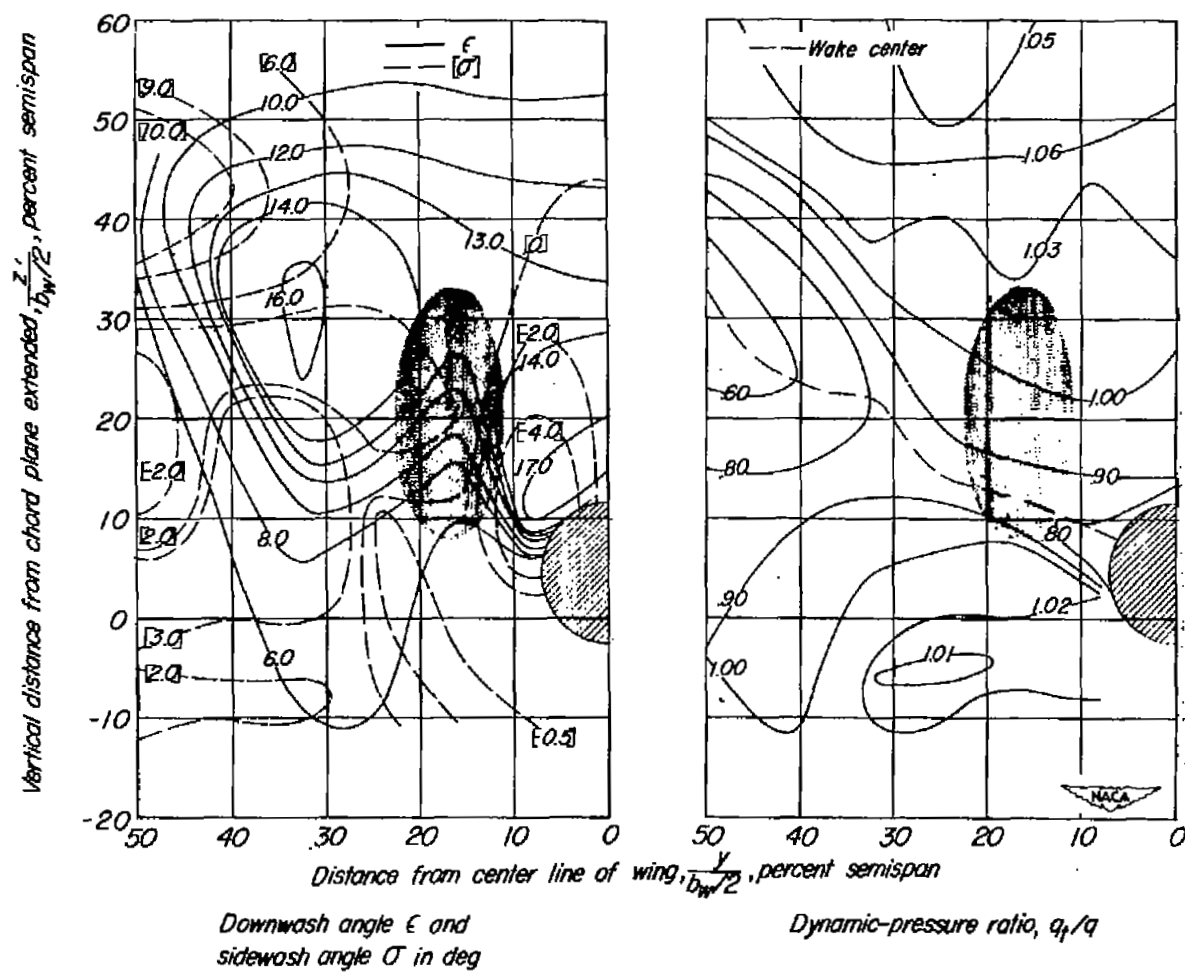
(b) $\alpha = 8.6^\circ$.

Figure 26.- Continued.



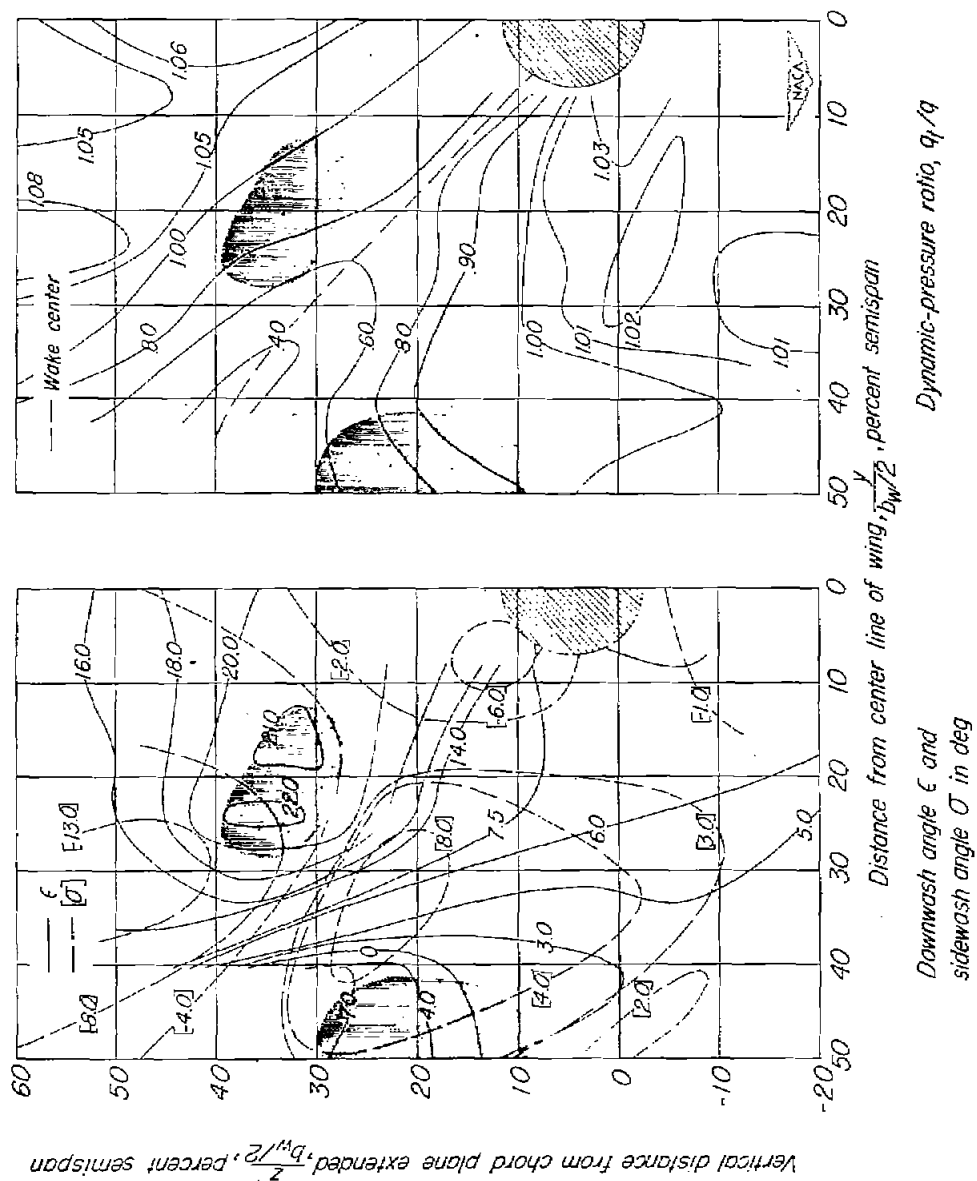
(c) $\alpha = 15.0^\circ$.

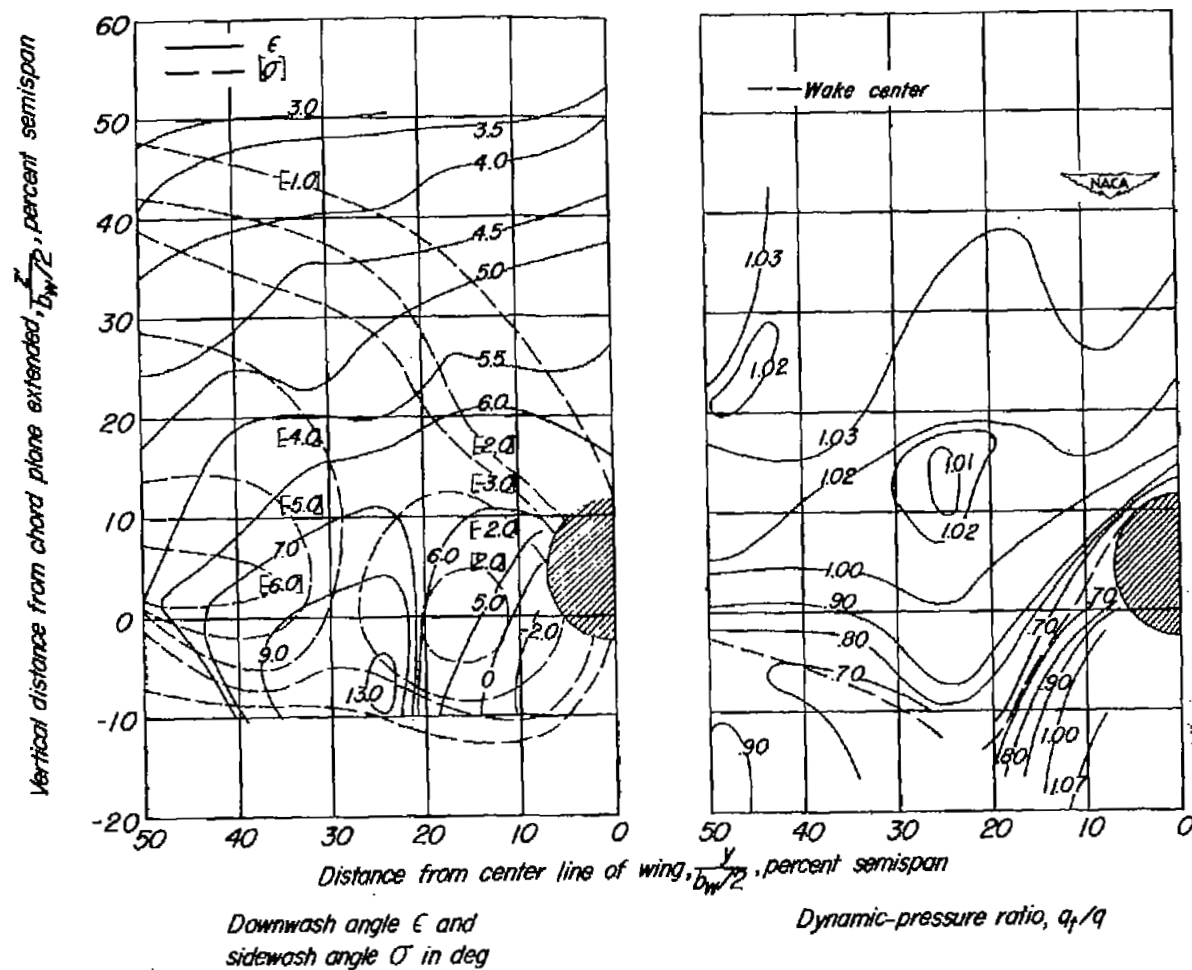
Figure 26.- Continued.



(d) $\alpha = 19.1^\circ$.

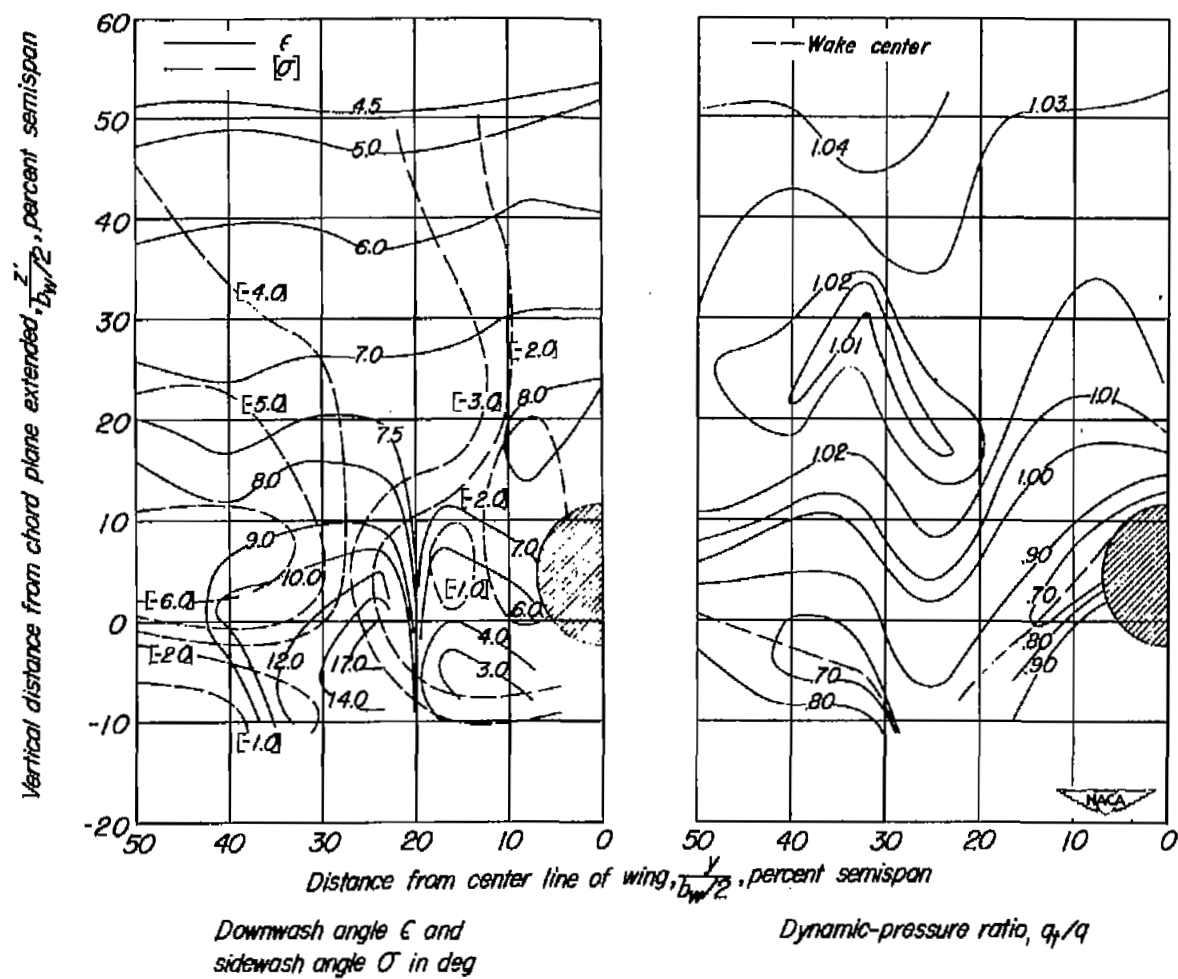
Figure 26.- Continued.





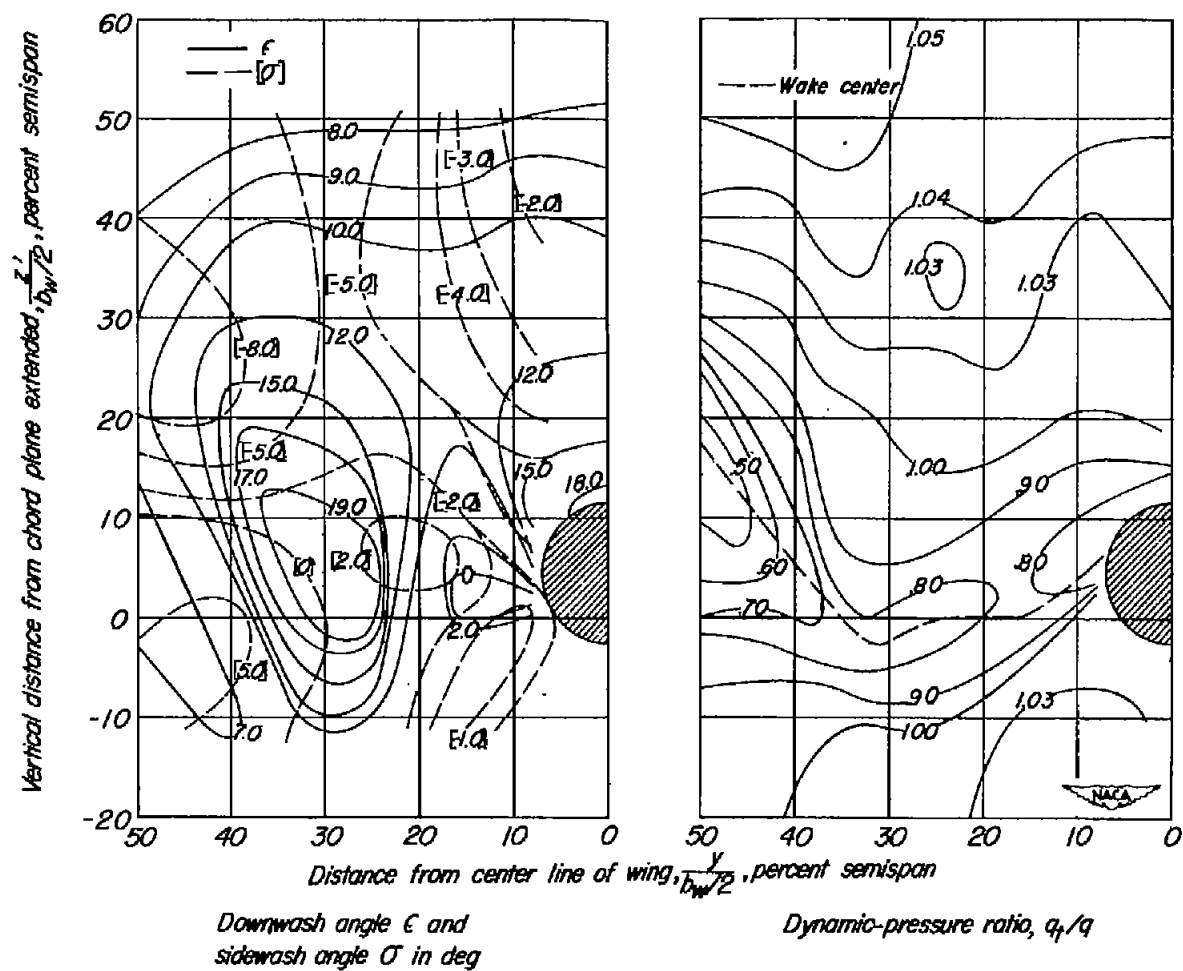
(a) $\alpha = 4.6^\circ$.

Figure 27.- Contour charts of the air-flow characteristics in the region of the horizontal tail. $0.475b/2$ leading-edge flaps and $0.400b/2$ split flaps; aspect ratio, 5.1; $R = 6.0 \times 10^6$. Shaded areas indicate extrapolated data.



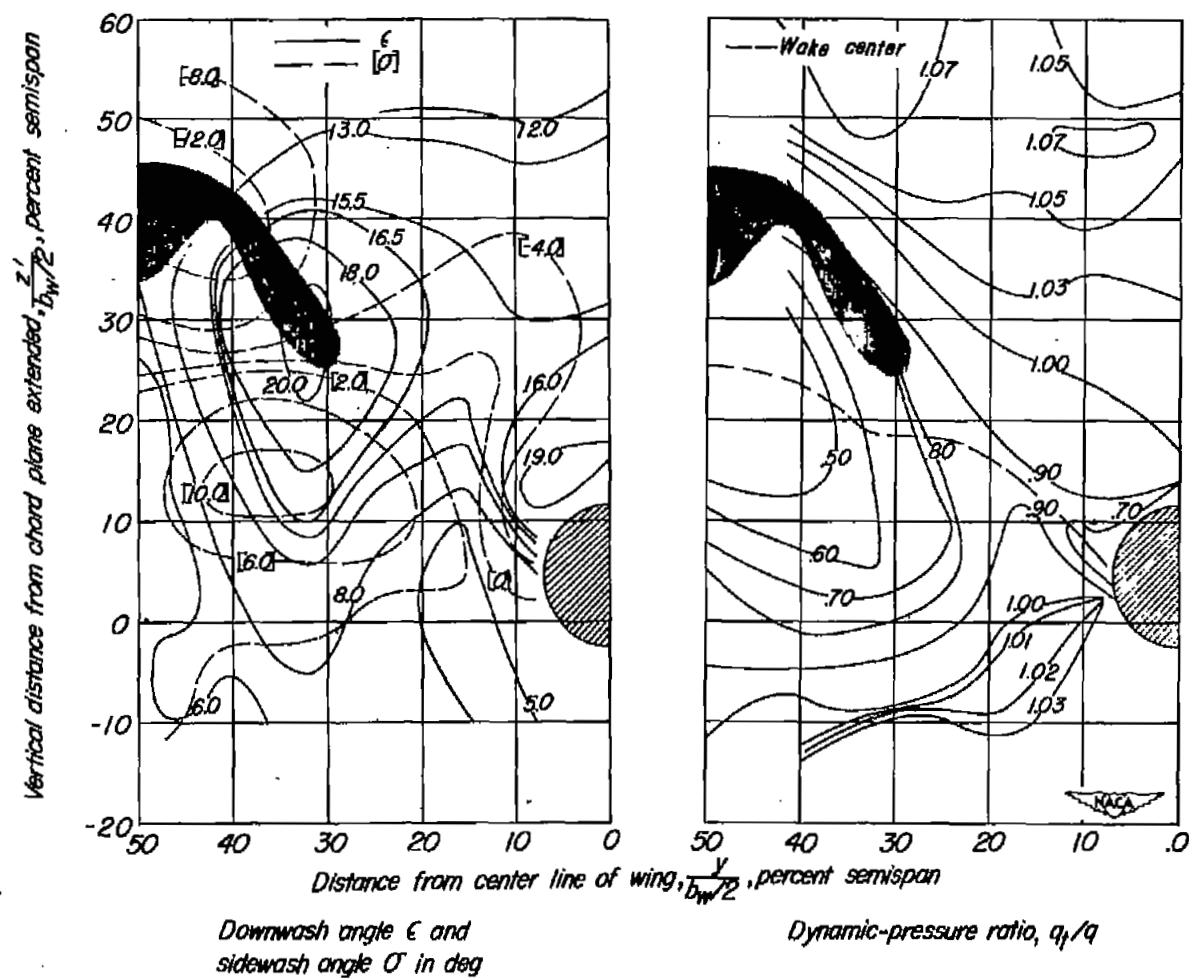
(b) $\alpha = 8.8^\circ$.

Figure 27.- Continued.



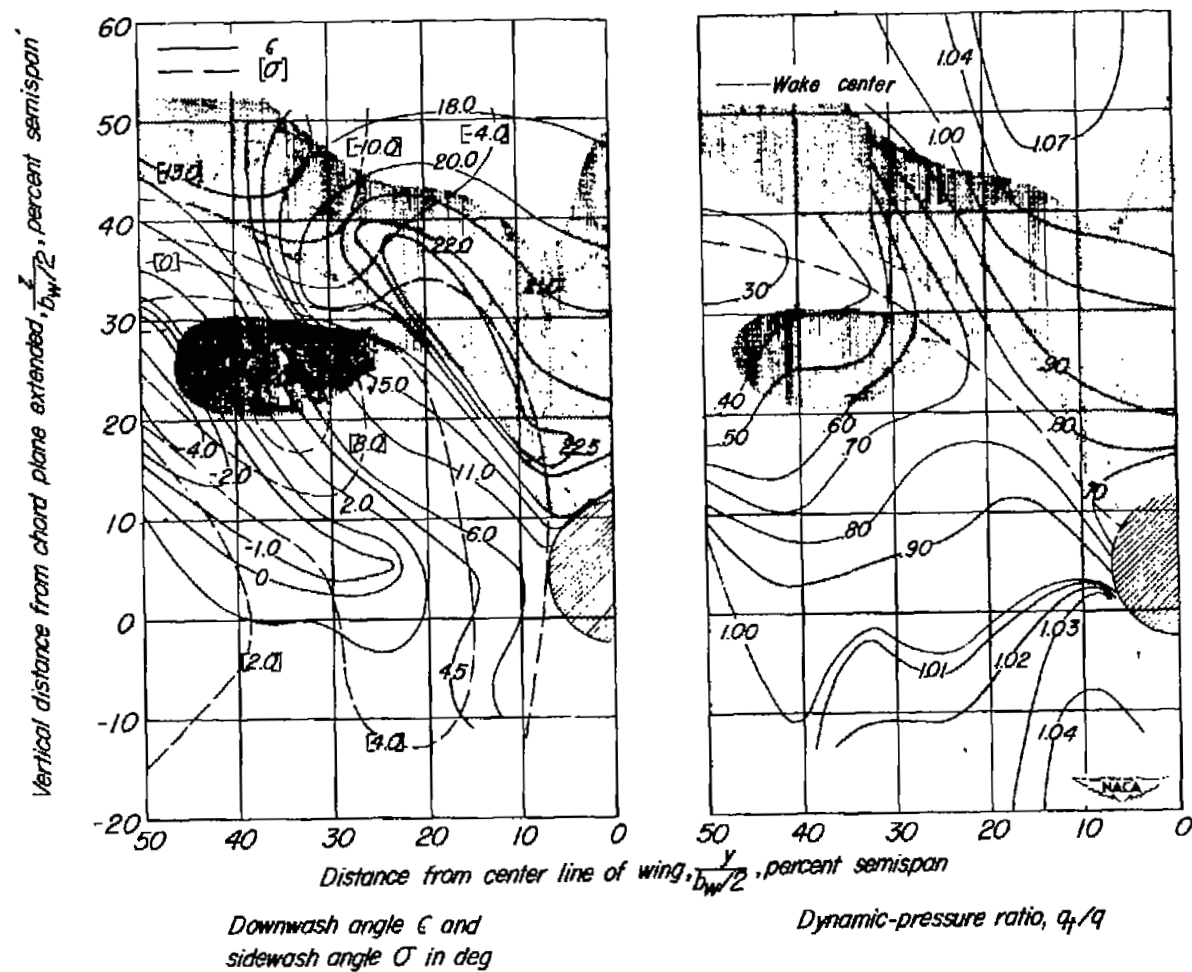
(c) $\alpha = 15.1^\circ$.

Figure 27.- Continued.



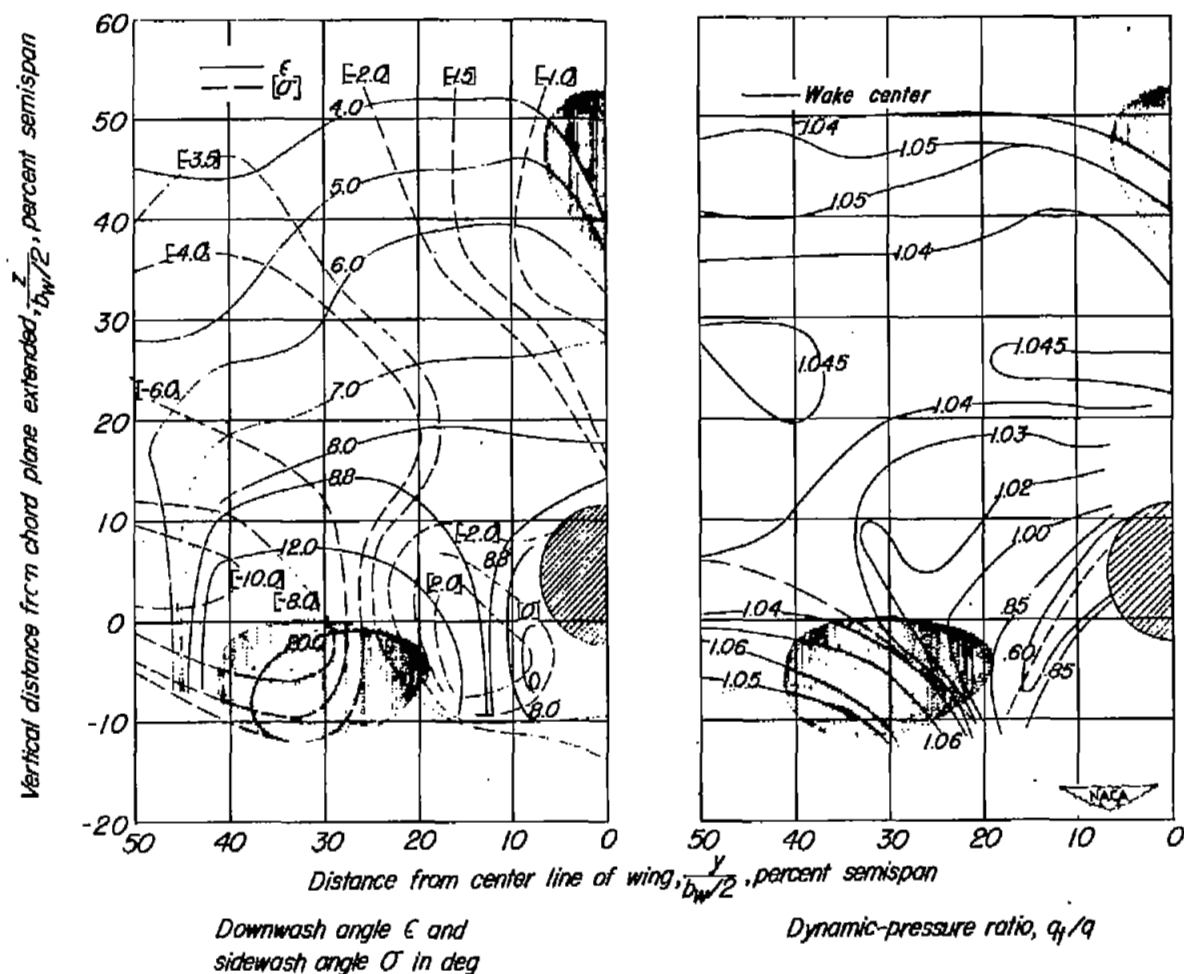
(d) $\alpha = 19.2^\circ$.

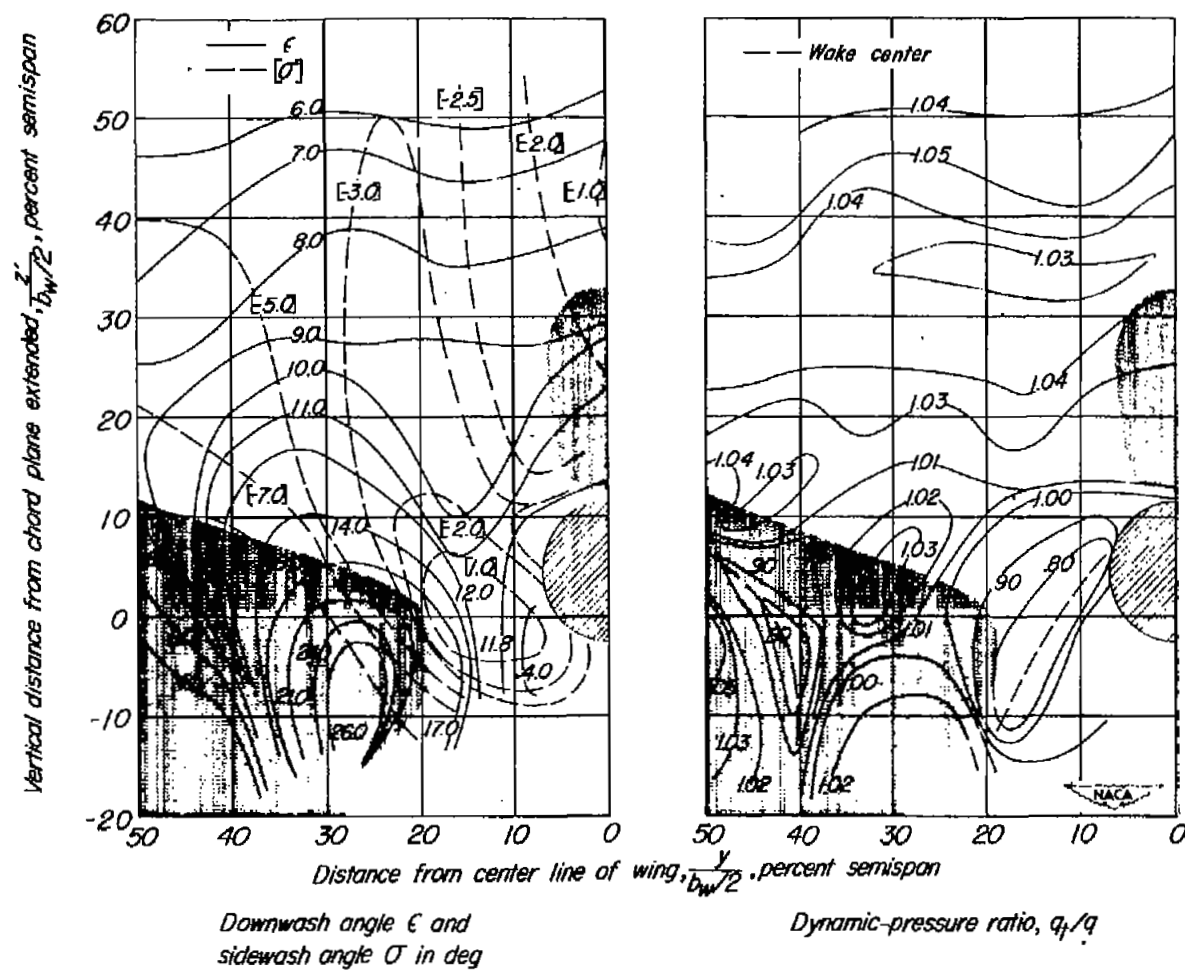
Figure 27.- Continued.



(e) $\alpha = 23.3^\circ$.

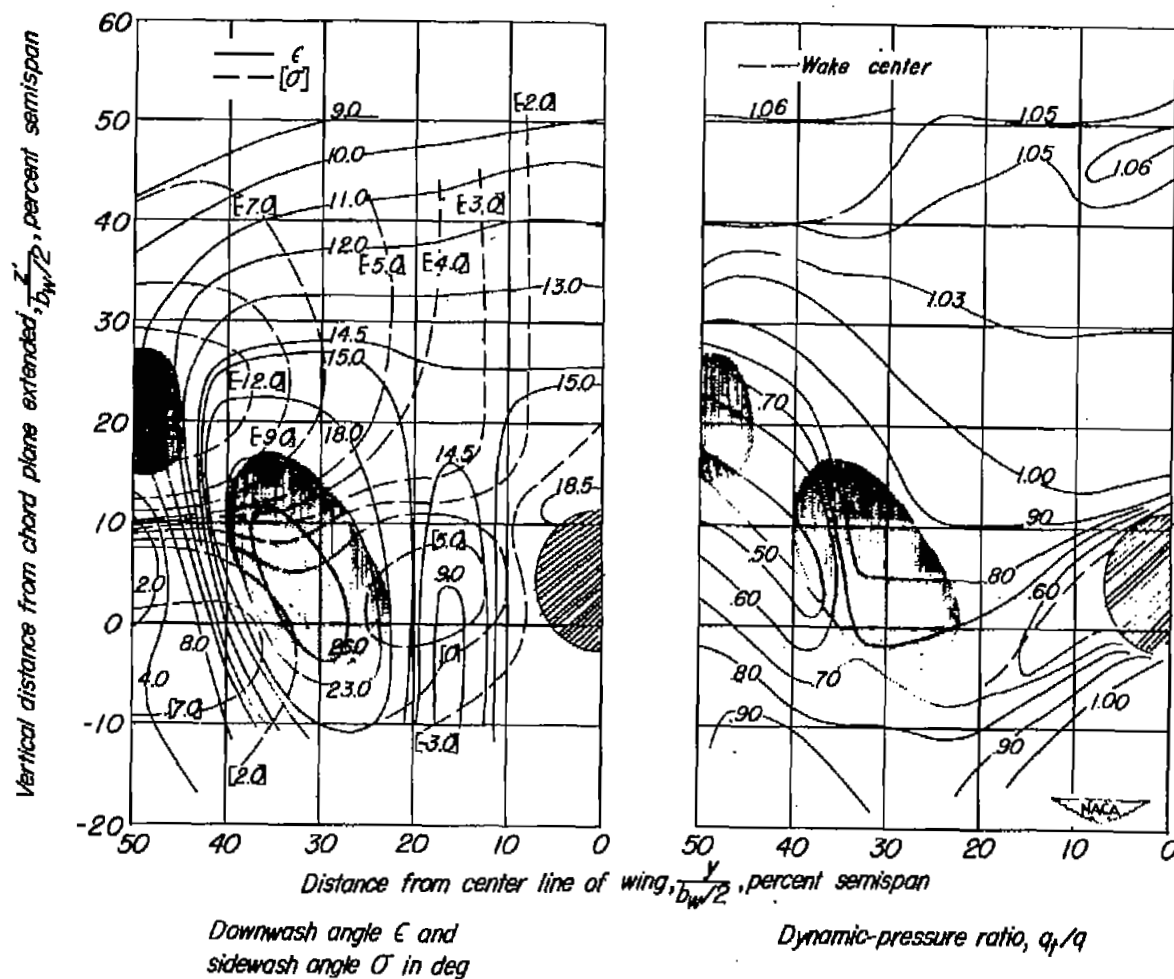
Figure 27.- Concluded.





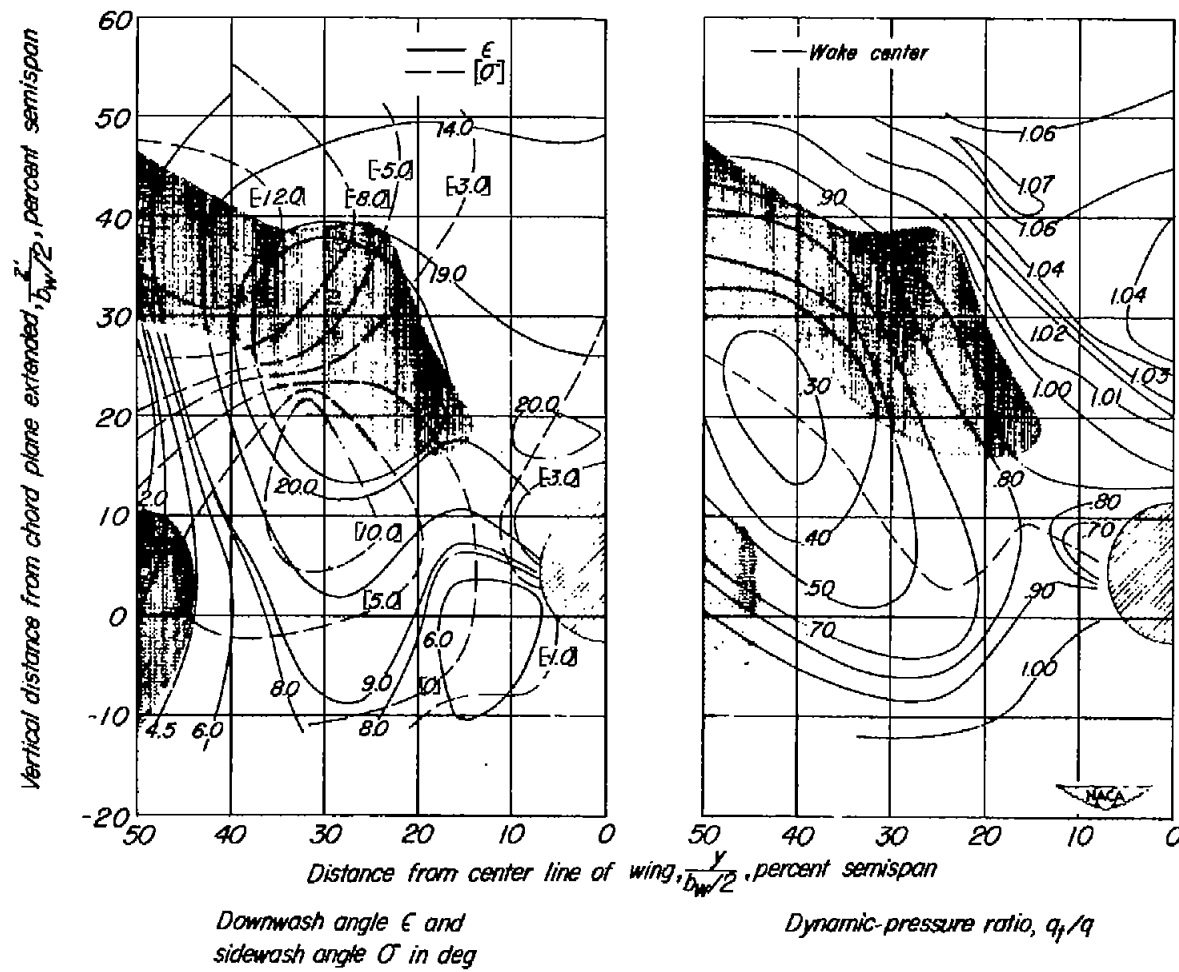
(b) $\alpha = 9.0^\circ$.

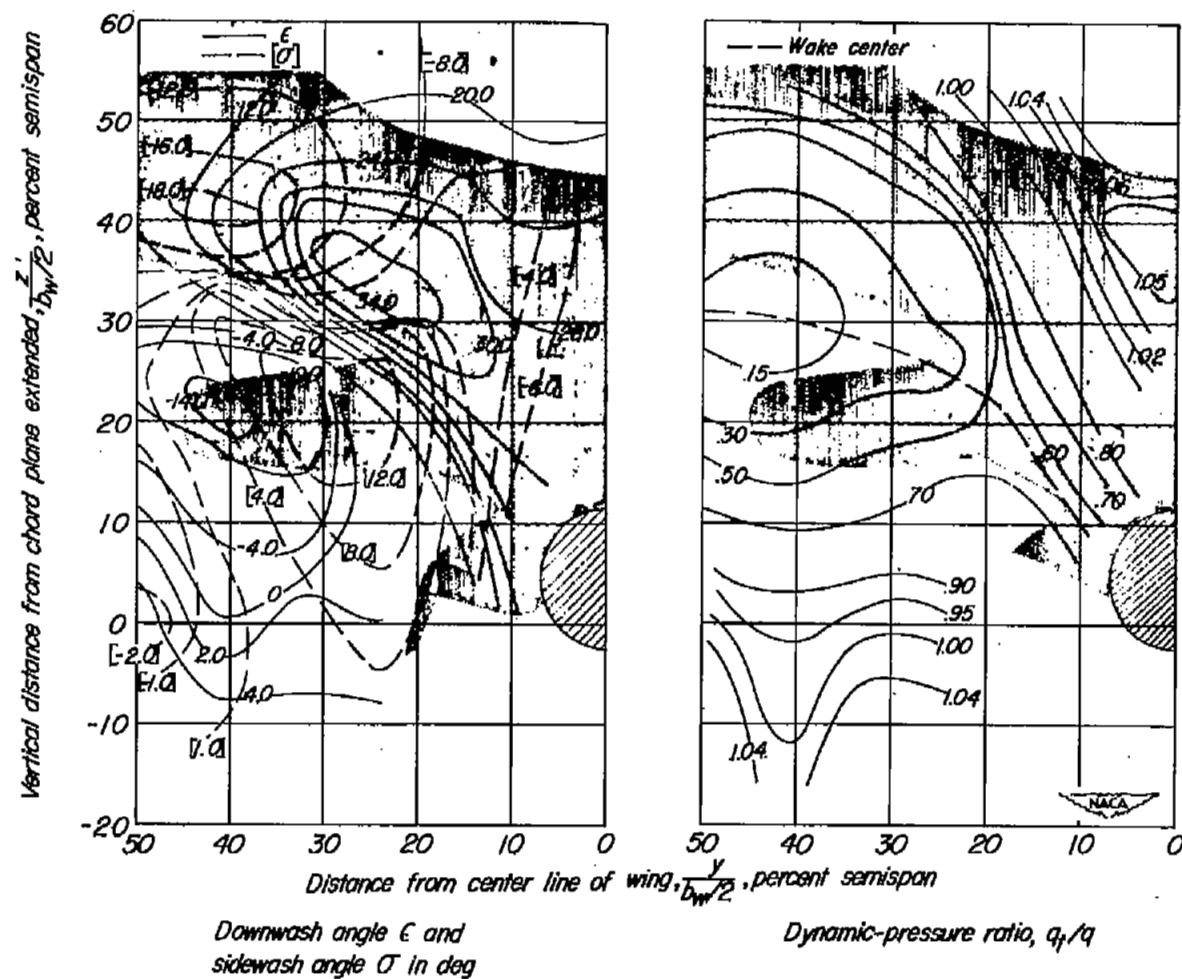
Figure 28.- Continued.



(c) $\alpha = 15.3^\circ$.

Figure 28.- Continued.





NASA Technical Library



3 1176 01436 2520